A Novel Rapid Host Cell Entry Pathway Determines Intracellular Fate of *Staphylococcus aureus*

Marcel Rühling[1], Fabio Schmelz[1], Kim Ulbrich[1], Fabian Schumacher[2], Julia Wolf[1], Maximilian Pfefferle[1], Magdalena Priester[1], Adriana Moldovan[1], Nadine Knoch[1], Andreas Iwanowitsch[1], Christian Kappe[3], Kerstin Paprotka[2], Burkhard Kleuser[2], Christoph Arenz[3], and Martin J. Fraunholz[1+]

[1]Chair of Microbiology, Julius-Maximilians-University Würzburg, Theodor-Boveri-Weg, 97074 Würzburg, Germany

[2]Institute of Pharmacy, Freie Universität Berlin, Königin-Luise-Straße 2+4, 14195 Berlin, Germany

[3]Institut for Chemistry, Humboldt Universität zu Berlin, Brook-Taylor-Str. 2, 12489 Berlin, Germany

[+]Corresponding author: martin.fraunholz@uni-wuerzburg.de

Abstract:

Staphylococcus aureus is an opportunistic pathogen causing severe diseases. Recently, *S. aureus* was recognized as intracellular pathogen, whereby the intracellular niche promotes immune evasion and antibiotic resistance. Interaction of *S. aureus* with versatile host cell receptors was described previously, suggesting that internalization of the pathogen can occur via several pathways. It remains elusive whether the pathway of internalization can affect the intracellular fate of the bacteria. Here, we identified a mechanism governing cellular uptake of *S. aureus* which relies on lysosomal Ca^{2+}, lysosomal exocytosis and occurs concurrently to other well-known entry pathways within the same host cell population. This internalization pathway is rapid and active within only few minutes after bacterial contact with host cells. Compared to slow bacterial internalization, the rapid pathway demonstrates altered phagosomal maturation as well as translocation of the pathogen to the host cytosol and ultimately results in different rates of intracellular bacterial replication and host cell death. We show that these alternative infection outcomes are caused by the mode of bacterial uptake.

Introduction

Sphingolipids are important components of eukaryotic membranes and also serve as bioactive signaling molecules (1). The most abundant sphingolipid, sphingomyelin (SM), resides in the extracellular leaflet of the plasma membrane and hence is exposed to the environment (2, 3). SM is a substrate for sphingomyelinases (SMases) that cleave off the phosphocholine head group to produce ceramide. Acid sphingomyelinase (ASM) is a lysosomal enzyme involved in recycling of SM (4, 5). Several studies demonstrated that ASM can be released by human cells either by Ca^{2+}-dependent liberation of lysosomal content via so called lysosomal exocytosis (6-8) or by channeling the enzyme through the Golgi secretory pathway (9, 10). Extracellular ASM is active on the plasma membrane, where it has important roles during repair of membrane wounds (6, 11) but has also been shown to act on the SM-containing low-density lipoprotein (12). The release of ASM through lysosomal exocytosis mediates host cell entry of several human pathogens (7, 8, 13-17).

Staphylococcus aureus is a Gram-positive human commensal that asymptomatically colonizes about one third of the human population (18). It is an opportunistic pathogen causing diseases ranging from soft tissue and skin infections (19) to lethal diseases (20, 21). *S. aureus* is notorious for acquiring antibiotic resistances thereby causing >100,000 annual (22). The pathogen possesses intracellular virulence strategies (23, 24) which contribute to antibiotic resistance (25, 26) and immune evasion (27). Internalization of *S. aureus* by host cells is mediated by several adhesins on the staphylococcal surface that bind a plethora of receptors on the host cell plasma membrane (13, 28-38). For instance, staphylococcal fibronectin-binding proteins that form fibronectin bridges to $\alpha_5\beta_1$ integrins on host cells to initiate internalization (28) or clumping factor B which can interact with the host receptor annexin A2 (31).

After internalization, *S. aureus* resides within a phagosome-like compartment that matures by acquiring proteins associated with early and then late endosomes as well as lysosomes (39-41). In epithelial and endothelial cells, the bacteria translocate to the host cytosol ["phagosomal escape", (39, 42, 43)]. Phagosomal escape is mediated by so-called phenol-soluble modulins (42), which comprise a family of helical amphiphilic peptides and are transcriptionally controlled by the accessory gene regulator *agr*, a staphylococcal quorum sensing system (44). *S. aureus* replicates in the host cytosol and cause host cell death for example by expression of a cysteine protease. (45).

The mechanism of pathogen entry into host cells has been suggested to dictate the outcome of infections (46-49). For instance, phagosomes formed during natural internalization of *Brucella abortus* by macrophages exhibited different characteristics compared to phagosomes that were artificially generated by phorbol myristate acetate (49). The protozoan parasite *Toxoplasma gondii* actively invades its host cells. Phagosomes generated during this active invasion differed from those that were generated during Fc receptor-mediated uptake of antibody-coated parasites (48). Since previous observation connecting host cell entry and intracellular fate of pathogens were based on artificial induction of internalization, it is unclear whether pathogens can enter host cells within the same population via different naturally occurring mechanisms and if the entry route has a direct influence on the outcome of an intracellular infection.

Here, we describe the internalization of *S. aureus* by tissue cells via a rapid pathway taking place within minutes after contact between bacteria and host cell surface. This pathway requires nicotinic acid adenosine dinucleotide phosphate (NAADP)-dependent mobilization of lysosomal Ca^{2+}, followed by lysosomal exocytosis and thereby release of ASM. Since the rapid uptake is concurrent to previously described internalization pathways, it probably has been missed due to long infection times used in traditional infection protocols [e.g., (28, 31, 35, 36)].

S. aureus bacteria, which enter host cells of the same cell population via the rapid pathway, cause a distinct infection outcome with altered phagosome maturation, bacterial translocation to host cytosol and eventually host cell death when compared to bacteria that enter host cells at later time points during infection. Thus, the outcome of an infection is decided at the single cell level during bacterial uptake at

the host plasma membrane. Bacteria-containing phagosomes that were formed by the ASM-dependent rapid uptake pathway are delayed in their maturation and the bacteria do not escape these organelles efficiently, hence demonstrating a direct link between concurrently active modes of bacterial uptake and the resulting outcomes of intracellular *S. aureus* infection.

Results

S. aureus triggers lysosomal Ca^{2+} mobilization for host cell invasion

We previously showed that internalization of *S. aureus* by host cells is associated with cellular Ca^{2+} signaling (50). To validate these findings, we treated human microvascular endothelial cells (HuLEC, **Figure 1**, A) or HeLa (**Supp. Figure 1**, A) with the cell permeant Ca^{2+} chelator BAPTA-AM (51) to interfere with host cell Ca^{2+} signaling and subsequently infected the cells with *S. aureus*. We measured the number of internalized *S. aureus* and determined the invasion efficiency by normalizing bacteria numbers detected in treated samples to untreated controls (set to 100%). Invasion efficiency was reduced by BAPTA-AM in a concentration-dependent manner, indicating an involvement of Ca^{2+} in the host cell entry process of *S. aureus*.

The cytosolic Ca^{2+} levels, which are crucial for signaling processes, can be elevated by Ca^{2+} influx from the extracellular space. To test whether *S. aureus* internalization is mediated by Ca^{2+} influx, we measured invasion efficiency, in absence of Ca^{2+} from the cell culture medium (**Figure 1**, A and **Supp. Figure 1**, A). Internalization of *S. aureus* by host cells was not affected by absence of Ca^{2+} ("Ca^{2+}-free, 0 µM BAPTA-AM"), thereby excluding a Ca^{2+} influx as crucial for *S. aureus* host cell entry. The pore-forming staphylococcal α-toxin was shown to mediate Ca^{2+} influx into host cells (11). *S. aureus* invasion into host cells was largely independent of the production of α-toxin (**Supp. Figure 1**, B), which further supported that the internalization is independent from extracellular Ca^{2+}.

Since intracellular Ca^{2+} stores, such as the ER or lysosomes, can serve as alternative source of Ca^{2+} (52), we next blocked Ca^{2+} liberation either from the ER using 2-APB (53) or 8-Bromo-cyclic ADP ribose (8-Bromo-cADPR; (54)) or from lysosomes using *trans*-Ned19 (55). Interference with lysosomal but not ER Ca^{2+} release reduced internalization of *S. aureus* in HuLEC (**Figure 1**, B) or HeLa (**Supp. Figure 1**, C, D) at concentrations which do not affect bacterial viability (**Supp. Figure 1**, E and F).

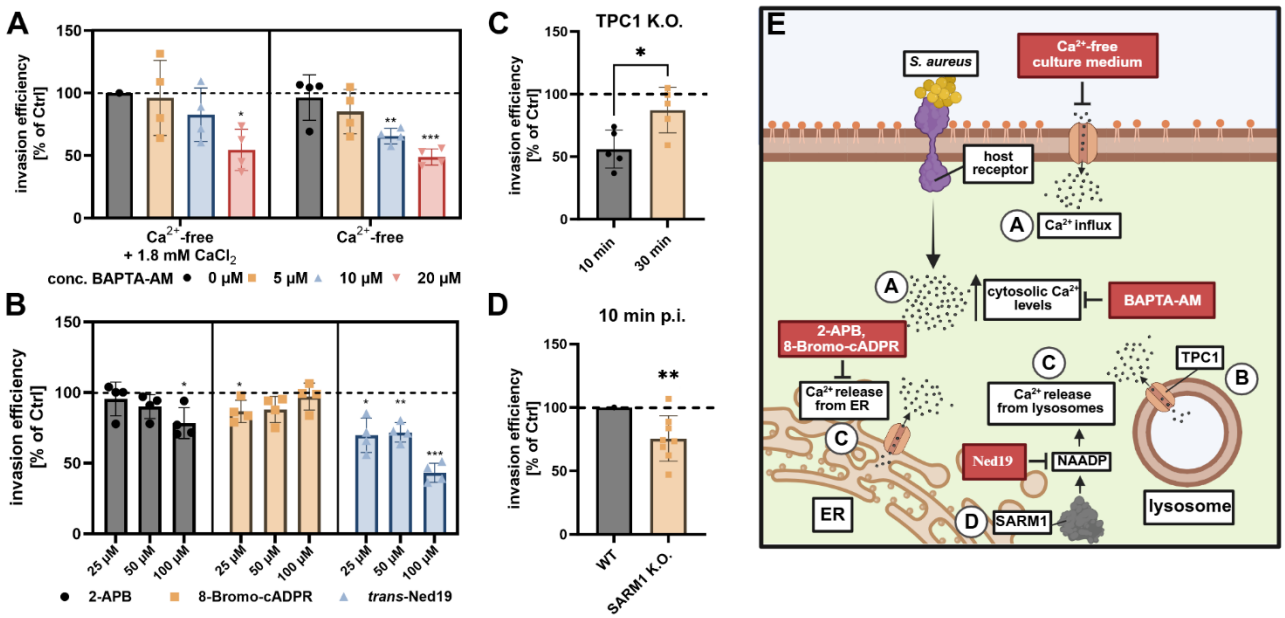

Figure 1 *S. aureus* invasion is dependent on Ca^{2+} liberation from lysosomal stores. Treatment with , BAPTA-AM (A, n≥4), *trans*-Ned19 (B, n≥4), but not 2-APB and 8-Bromo-cADPR (B, n≥4) reduce *S. aureus* internalization by host cells. Genetic ablation of TPC1 (C, n=5) and SARM1 (D, n=8) reduced invasion of *S.*

aureus 10 min p.i . HuLEC (A, B), HeLa WT (C, D), HeLa TPC1 K.O. (C) or HeLa SARM1 K.O. (D) cells were treated with the respective substance and were subsequently infected with *S. aureus* JE2 for 30 min if not indicated otherwise. Extracellular bacteria were removed by lysostaphin, and the number of intracellular bacteria was determined by CFU counting. Results were normalized to untreated controls to obtain invasion efficiency (in percent of control). (F) Scheme of host cell Ca^{2+} signaling and interfering agents. Letters indicate figure panels that supported the respective conclusion. Statistics: one sample t-test (A, B,D,), unpaired Student´s t-test (C). Bars represent means ± SD. *p≤0.05, **p≤0.01, ***p≤0.001, ****p≤0.0001.

Ned19 antagonizes NAADP, a second messenger that mediates opening of two pore channels (TPCs), which transport Ca^{2+} from the endo-lysosomal compartment into the cytosol (55). Hence, a HeLa cell pool depleted of TPC1 (**Supp. Figure 1***,* G) showed substantially reduced invasion when compared to wildtype HeLa cells. This was particularly pronounced after a 10 min infection pulse, suggesting that Ca^{2+}-dependent invasion is important early in infection (**Figure 1**, C).

CD38 is a well-known producer of NAADP in immune cells (56-58). Thus, we tested *S. aureus* invasion in HeLa cells treated with the specific CD38 inhibitor 78c, even though expression of CD38 in these cells is predicted to be very low (proteinatlas.org). We observed no effect on *S. aureus* invasion by CD38 inhibition (**Supp. Figure 1**, H). An alternative NAADP producer, with higher expression in our infection model, is *Sterile Alpha and TIR Motif Containing 1* [SARM1, (59)]. We measured a slightly decreased invasion efficiency 10 min p.i. in a cell pool lacking SARM1 when compared to wildtype cells (**Figure 1**, D; **Supp. Figure 1**, I), suggesting that SARM1 might be involved in NAADP production during internalization of *S. aureus* by host cells. However, there might be other enzymes that produce NAADP (60) during *S. aureus* infection.

Altogether, our findings show that interference with lysosomal Ca^{2+} mobilization limits *S. aureus* invasion particularly early in infection.

S. aureus invasion requires lysosomal exocytosis, ASM and its substrate sphingomyelin on the host cell surface

Since our data suggest that lysosomal Ca^{2+} release facilitates the internalization of *S. aureus* by host cells, we speculated that lysosomal exocytosis is involved in bacterial invasion. Lysosomal exocytosis is a Ca^{2+}-dependent process during which lysosomes fuse with the plasma membranes and release their content. The internalization of several human pathogens has been shown to depend on lysosomal exocytosis (8, 16, 61-63).

To visualize lysosomal exocytosis, we developed an assay that makes use of the split NanoLuc luciferase system [**Figure 2**, A; (64, 65)]. We here engineered HeLa cells to express the high-affinity NanoLuc peptide HiBiT between the signal peptide and the mature chain of lysosomal-associated membrane protein 1 (LAMP1). Transient localization of LAMP1 to the cell surface of mammalian cells is a hall mark for lysosomal exocytosis (66). To measure the release of the HiBiT-tagged LAMP1, we added LgBit together with the NanoLuc substrate Furimazine to the cell culture medium and measured luminescence of reconstituted NanoLuc in a microplate reader. Maximum luminescence was detected ~10-15 min upon starting the assay and decline afterwards, likely due to exhaustion of the luciferase substrate (**Figure 2**, B). Treatment with the Ca^{2+} ionophore ionomycin, a known activator of lysosomal exocytosis (11, 67), increased the luminescence, whereas Vacuolin-1, an inhibitor of lysosomal exocytosis (68), decreased luminescence when compared to an untreated control. Thus, we concluded that our assay successfully quantified exposure of LAMP1 on the host cell surface.

Next, we monitored LAMP1 surface levels during *S. aureus* infection. We assumed that ionomycin would trigger exocytosis of all "releasable" lysosomes. Hence, the detected luminescence signal during infection was scaled to an untreated control (=0 %) as well as ionomycin (=100%), to express LAMP1 surface levels as percentage of all "releasable" lysosomes. We detected that ~30% of all "releasable" lysosomes were liberated from the reporter cells 10 min after infection with *S. aureus* (**Figure 2**, C). Pretreatment of host cells with Vacuolin-1 or Ned-19 strongly reduced LAMP1 surface levels,

suggesting that *S. aureus* triggers lysosomal exocytosis in an NAADP-dependent manner during invasion.

To test whether lysosomal exocytosis is required for *S. aureus* internalization by host cells, we measured invasion efficiency in HuLEC (**Figure 2**, D) and HeLa cells (**Supp. Figure 2**, A) pretreated with Vacuolin-1. Invasion was strongly reduced in inhibitor-treated samples, while the survival of the bacteria was not affected by the compound (**Supp. Figure 2**, B).

Next, we triggered lysosomal exocytosis in HuLEC by addition of ionomycin prior to infection, thereby depleting the pool of "releasable" lysosomes and thus preventing lysosomal exocytosis during infection. Ionomycin pretreatment reduced invasion efficiency in a concentration-dependent manner (**Figure 2**, E). Bacterial growth and survival as well as host cell integrity were not affected at the concentrations used (1 µM, **Supp. Figure 2**, C-E).

Synaptotagmin 7 (Syt7) is known to support fusion of lysosomes with the plasma membrane in a Ca^{2+}-dependent manner (69). Accordingly, Syt7-depleted HeLa cells demonstrated lower bacterial invasion (**Figure 2**, F). As already observed for TPC1 (**Figure 1**, C), this was most pronounced early in infection. Taken together, our results support the hypothesis that lysosomal exocytosis is important for invasion of host cells by *S. aureus* particularly early during infection.

Lysosomal exocytosis results in release of ASM (6, 11), an enzyme which has previously been associated with the internalization of several bacterial and viral pathogens (8, 13, 16, 62, 63, 70) and thus, we tested if ASM activity is also required for the uptake of *S. aureus* by host cells. Therefore, we treated different cell lines prior to infection with amitriptyline, a functional inhibitor of ASM (FIASMA), or the competitive ASM inhibitor ARC39 (71) and infected host cells with *S. aureus*. While invasion in HuLEC, human umbilical vein endothelial cells (HuVEC) and HeLa was reduced by both inhibitors, invasion in bronchial epithelial $16HBE14o^{-}$ and the endothelial-epithelial hybrid cell line EA.hy926 was not or only marginally altered (**Figure 2**, G). The used inhibitor concentrations did not affect bacterial survival (**Supp. Figure 2**, F, G). Furthermore, we excluded that differences among cell lines arose from differential ASM activity or sensitivity to the inhibitors by monitoring enzymatic activity [**Supp. Figure 2**, H; (72) and **Supp. Figure 2**, I; (73)].

Next, we treated HuLEC with 10 µM ARC39 or 0.5 µM PCK310, a fast-acting ASM inhibitor. Already after 1h preincubation, PCK310 reduced invasion of *S. aureus*, whereas ARC39 required overnight treatment for a similar reduction (**Figure 2**, H). We confirmed the reduction of internalized colony forming units (CFU) by amitriptyline and PCK310 treatment with a microscopy-based approach, where we determined the number of invaded fluorescent bacteria per host cell (**Supp. Figure 2**, J).

Taking together, our results show that ASM is involved in *S. aureus* invasion of host cells in a cell-type specific manner.

Next, we generated two ASM-depleted HeLa cell pools using CRISPR/Cas9 (74) with two distinct small guide RNAs (sgRNAs) and determined successful ablation of cellular ASM activity with a visible range ASM FRET probe [(73), **Supp. Figure 2**, K]. Surprisingly, we did not detect a reduced invasion efficiency in ASM K.O. cells, when compared to wildtype (**Figure 2**, I). To test if unspecific side effects of the ASM inhibitors could have contributed to reduced invasion in our previous experiments, we treated wildtype and ASM K.O.s with ARC39 and tested for *S. aureus* invasion efficiency (**Figure 2**, K). In wildtype cells, bacterial invasion again was strongly reduced after ARC39 treatment, whereas only a slight reduction was observed in the K.O.s, which may represent unspecific side effects of the inhibitor. Since the reducing effect of ARC39 on invasion is almost completely lost in ASM K.O. cells, the reduced invasion in wildtype cells upon ARC39 treatment predominantly must be caused by the inhibition of ASM.

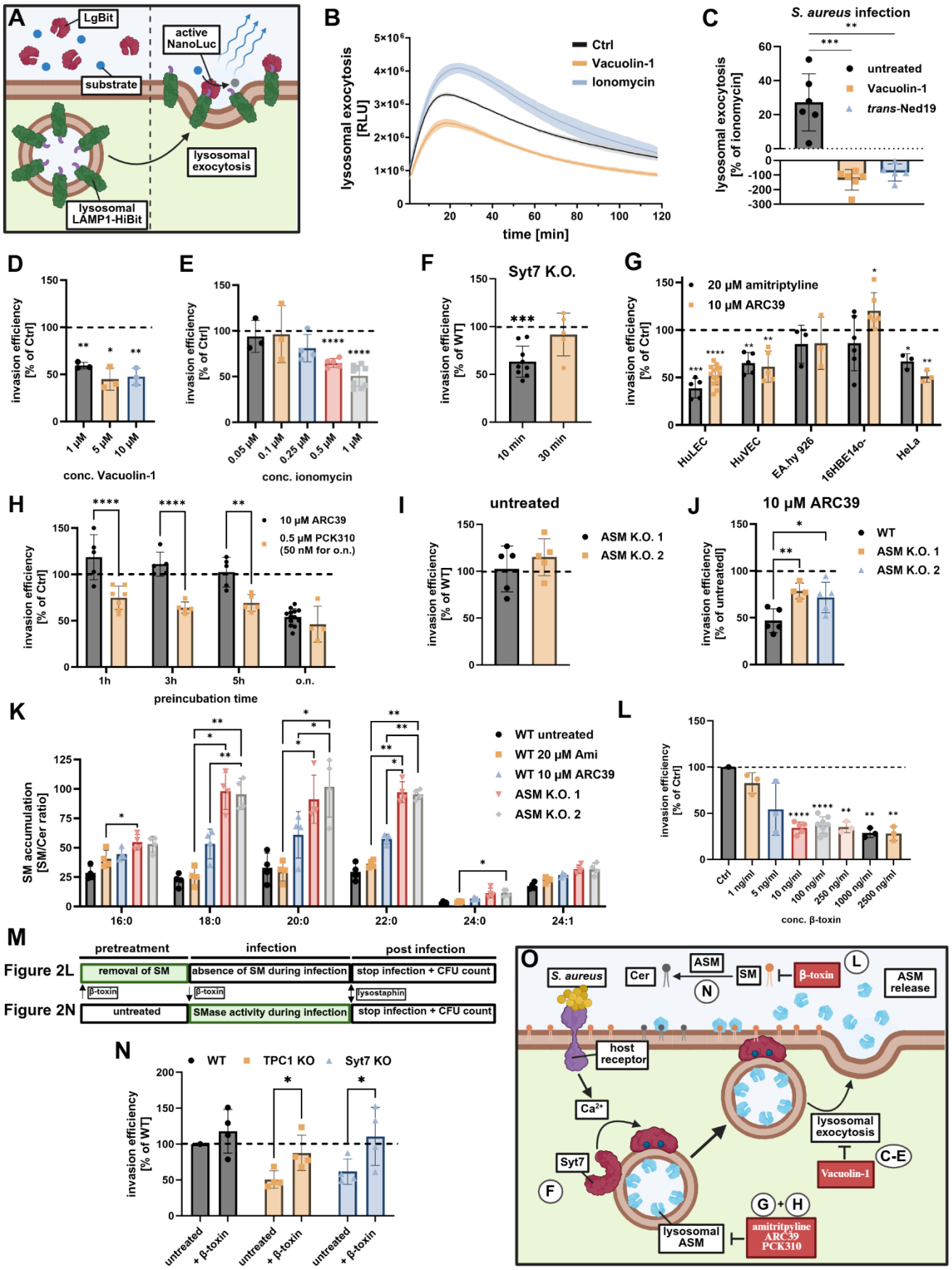

Figure 2 *S. aureus* invasion requires lysosomal exocytosis, ASM and plasma membrane sphingomyelin.
(A, B) Luminescence-based lysosomal exocytosis assay. HeLa cells expressing LAMP1-HiBit were treated with 1 µM ionomycin (immediately before the measurement) or 1 µM Vacuolin-1 (75 min before the measurement) in

presence of LgBit and NanoLuc substrate. Lysosomal exocytosis was monitored by measuring chemiluminescence in a Tecan microplate reader. n=3 **(C) *S. aureus* triggers lysosomal exocytosis during infection.** HeLa cells expressing LAMP1-HiBit were pretreated for 75 min with 1 µM Vacuolin-1 or 200 µM *trans*-Ned19. Subsequently, cells were infected with *S. aureus* JE2 (MOI10), treated with 1 µM ionomycin or left untreated and lysosomal exocytosis was determined by measuring chemiluminescence in a Tecan microplate reader 10 min p.i. Luminescence detected in infected samples was scaled to untreated controls (0 %) and ionomycin (100%) to determine the proportion of all "releasable" lysosomes liberated during infection. n=6. **(D-F) *S. aureus* invasion requires Syt7-dependent lysosomal exocytosis.** HuLEC were treated with the lysosomal exocytosis inhibitor Vacuolin-1 or the lysosomal exocytosis inducer ionomycin and invasion efficiency of *S. aureus* was determined 30 min p.i. (D, E, n≥3). Invasion efficiency of *S. aureus* JE2 was determined in HeLa Syt7 K.O. cells 10 min and 30 min p.i. (F, n≥5; data normalized to HeLa wildtype). **(G, H) *S. aureus* internalization is dependent on ASM activity in endothelial and epithelial cells.** Indicated cell lines were treated with the ASM inhibitors amitriptyline or ARC39 (G) and invasion efficiency of *S. aureus* was determined (n≥3). (G) HuLEC were treated with PCK310 or ARC39 for the indicated periods. Subsequently, cells were infected with *S. aureus* for 30 min and invasion efficiency was determined by CFU counting (H). n≥4. **(I, J) Genetic ablation of ASM renders *S. aureus* invasion insensitive towards ARC39.** HeLa ASM K.O. cells were treated with 10 µM ARC39 or were left untreated and the number of invaded bacteria was determined 30 min p.i.. Invasion efficiency was determined by normalization to wildtype HeLa cells (I) or to corresponding untreated samples (J, n≥4), **(K) Genetic ablation of ASM is accompanied by massive alteration in cellular sphingolipid profiles.** HeLa wildtype and ASM K.O. cells were treated with 20 µM amitriptyline (75 min) and 10 µM ARC39 (22h) or left untreated, as indicated**.** Whole cell sphingolipid profiles were determined by HPLC-MS/MS and the ratios of SM vs. Cer were calculated for lipid species with varying acyl side chains (chain length indicated on the x-axis). n= 4 **(L) *S. aureus* invasion requires SM on host cell plasma membranes.** HuLEC were treated with the bacterial SMase β-toxin for 75 min and were subsequently infected with *S. aureus* JE2 for 30 min (n≥3). **(M) Experimental design for β-toxin treatment of host cells during *S. aureus* infection.** Host cells were either pretreated with β-toxin to remove SM from the plasma membrane prior to infection (upper panel; **Figure 2, L).** Alternatively, β-toxin was added together with the bacteria to rescue the absence of ASM (lower panel, **Figure 2, N)**. **(N) Presence of extracellular SMase activity restores the invasion defect in TPC1 and Syt7 K.O. cell lines.** HeLa wild type as well as TPC1 or Syt7 KO cell lines were infected with *S. aureus* JE2 in presence of 100 ng/ml of the bacterial SMase β-toxin and invasion efficiency 10 min p.i. was determined (n=4). In each experiment the numbers of intracellular *S. aureus* JE2 were determined by lysostaphin protection assay and CFU counting. Results obtained for the tested condition were normalized to the wildtype cell line or the mock-treated control. (**O) Scheme of lysosomal exocytosis and ASM release as well as interfering agents.** Cer: ceramide, SM: sphingomyelin, ASM: acid sphingomyelinase. xStatistics: one sample t-test (D-G, L), one-way ANOVA and Dunnett's multiple comparisons test (C, J). Mixed-effects model (REML) and Šídák's multiple comparisons (H). Two-way ANOVA and Tukey's multiple comparison (K). Two-way RM ANOVA and Šídák's multiple comparison (N) Bars represent means ± SD. *p≤0.05, **p≤0.01, ***p≤0.001, ****p≤0.0001.

Absence of ASM results in cellular accumulation of SM and usually is accompanied by the neurodegenerative diseases, Niemann-Pick syndrome A and B (75). Hence, we compared the sphingolipidomes of inhibitor-treated wildtype and ASM K.O. cells by high-pressure liquid chromatography coupled to tandem mass spectrometry (HPLC-MS/MS). The SM accumulation is described as ratio of cellular SM vs. ceramide concentrations (ASM educt vs. product) for lipid species with different acyl chain lengths (**Figure 2**, K). Whereas we did observe a moderately increased amount of most SM species upon ARC39 treatment, cells exposed to amitriptyline only showed a slight increase in SM 16:0, which can be explained by the shorter preincubation time used for amitriptyline (75 min vs. 22h). However, in both ASM K.O. cell lines we observed markedly increased SM levels when compared to either untreated or inhibitor-treated wildtype cells. The relatively low increase of SM levels after inhibitor treatment likely arises from short inhibitor pulses (in the range of minutes or hours), whereas SM in ASM K.O. cell lines accumulates over the entire culture period (days or weeks since gene ablation). We hypothesize that in the latter situation the host cell invasion of *S. aureus* is generally increased, while the ASM-dependent uptake pathway is absent. This is supported by the high residual internalization of *S. aureus* by ASM K.O. cells upon ARC39 treatment. Previously, it was shown that *S. aureus* host cell entry is limited by caveolin-1, a protein associated with lipid microdomains (76, 77). Absence of ASM was demonstrated to interfere with caveolin-1-associateded endocytosis (78, 79) and thus, the increased invasion in ASM K.O. cells may be caused by dysfunctional caveolin-1.

265 Release of ASM by host cells results in cleavage of SM on the host cell surface, a process that previously
266 was suggested to facilitate cell entry of human pathogens (7, 8, 13-17). To test whether *S. aureus*
267 invasion requires SMase activity on the host cell surface, we removed SM, the substrate of ASM, from
268 plasma membranes of HuLEC (**Figure 2**, L) and HeLa (**Supp. Figure 2**, L) by pretreatment with the
269 bacterial SMase β-toxin (see **Figure 2**, M). We confirmed β-toxin-dependent SM conversion in living
270 cells by detecting the ceramide metabolites of fluorescent SM analogs [**Supp. Figure 2**, M; (81)].
271 Plasma membrane pretreatment with bacterial SMase reduced *S. aureus* invasion efficiency in a
272 concentration-dependent manner in both cell lines. 10 ng/ml β-toxin were sufficient to decrease invasion
273 to ~30% of that measured in untreated control cells. Interestingly, a 250-fold higher concentration did
274 not lead to further reduction, suggesting that 10 ng/ml β-toxin were sufficient to quantitatively convert
275 SM to ceramide at the cell surface. In line with our previous experiments, this suggests that multiple *S.*
276 *aureus* invasion pathways exist within the same host cell population, of which at least one requires SM
277 and its enzymatic breakdown on the plasma membrane.
278 Since we detected enhanced Ned19-sensitive lysosomal exocytosis during *S. aureus* infection (**Figure**
279 **2**, C), we hypothesized that absence of TPC1 or Syt7 should impair lysosomal exocytosis and thereby
280 release of ASM. Therefore, we infected wildtype as well as TPC1 or Syt7 K.O. cells with *S. aureus* in
281 presence (but without pretreatment, see **Figure 2**, M) of 100 ng/ml β-toxin and determined the number
282 of intracellular bacteria after 10 min (**Figure 2***,* N). The addition of β-toxin to the culture medium
283 completely rescued the invasion defect of the K.O. cells. This indicates that reduced bacterial
284 internalization in absence of TPC1 and Syt7 results from a lack in ASM delivery to the cell surface by
285 Ca^{2+}-dependent lysosomal exocytosis and that absence of ASM from the host cell surface, can be
286 compensated by exogenous addition of the bacterial SMase β-toxin.
287 We want to emphasize the difference in experimental application of β-toxin (**Figure 2**, M) where we i)
288 pretreat host cells with the bSMase to remove SM from the plasma membrane (**Figure 2**, L and **Supp.**
289 **Figure 2**, L) and ii) rescue the absence of exocytosed ASM from the host cell surface by exogenous
290 addition of β-toxin during the infection (**Figure 2***,* N). In the former case, pretreatment leads to removal
291 of SM from the plasma membrane thus preventing SM conversion by ASM during infection and
292 resulting in reduced invasion. The latter leads to SM conversion by the bacterial SMase during infection
293 thereby increasing invasion.
294 In summary, our data suggest the existence of a *S. aureus* invasion pathway that depends on the
295 metabolic breakdown of SM by ASM on the host cell surface (**Figure 2**, O).
296
297 ***ASM- and Ca^{2+}-mediated invasion is rapid***
298 To study the role of SM in *S. aureus* uptake kinetics, we incubated HuLEC with fluorescent sphingolipid
299 analogs and recorded *S. aureus* infection by time lapse imaging [**Figure 3**, A; **Supp. Video 1**; **Supp.**
300 **Figure 3**; **Supp. Video 2**; (73)]. We observed that the bacteria were rapidly engulfed by SM-containing
301 membrane compartments. While association of bacteria with BODIPY-FL-C12-SM increased over time
302 during the first 30 min of infection, this was not observed for BODIPY-FL-C12-Ceramide, suggesting
303 that *S. aureus* invasion specifically relies on interaction with SM in host cell plasma membranes (**Figure**
304 **3**, B).
305 Next, we determined the invasion efficiency of *S. aureus* in a time-dependent manner and blocked
306 invasion by either ASM inhibitors, ionomycin, BAPTA-AM or β-toxin pretreatment. We found a time-
307 dependent increase in intracellular bacteria, whereby all treatment conditions reduced bacterial invasion
308 at every time point with the untreated control at 30 min set to 100% (**Figure 3**, C). We next normalized
309 the data to the untreated control of the corresponding time point. Except for the β-toxin treatment, the
310 effect of all other treatments was most pronounced early (5-10 min) after infection (**Figure 3**, D). For
311 instance, ionomycin treatment massively reduced *S. aureus* invasion to ~20% of untreated controls when
312 we infected for 10 min. We concluded that in untreated controls 80% of the bacteria entered host cells
313 via the pathway that depends on lysosomal exocytosis, Ca^{2+} and ASM, which is blocked by ionomycin

treatment. Consequently, bacteria that were able to invade host cells in ionomycin-treated samples (the residual ~20%) must have employed other pathways. By contrast, in samples infected for 30 min a higher proportion of bacteria was able to enter host cells despite ionomycin treatment (~50% compared to untreated controls). This suggests that only 50% of all invaded bacteria were internalized in an ASM- and Ca^{2+}-dependent fashion upon the longer infection pulse. Together with the observed invasion defects in host cells with gene deletions in TPC1 (**Figure 1**, C) and Syt7 (**Figure 2**, F), which we exclusively detected during short infection times, our data suggest that early during infection bacteria enter host cells predominantly in an ASM- and Ca^{2+}-dependent manner. Thus, we concluded that the internalization pathway that depends on lysosomal exocytosis, ASM and Ca^{2+} is rapid when compared to other host cell entry pathways.

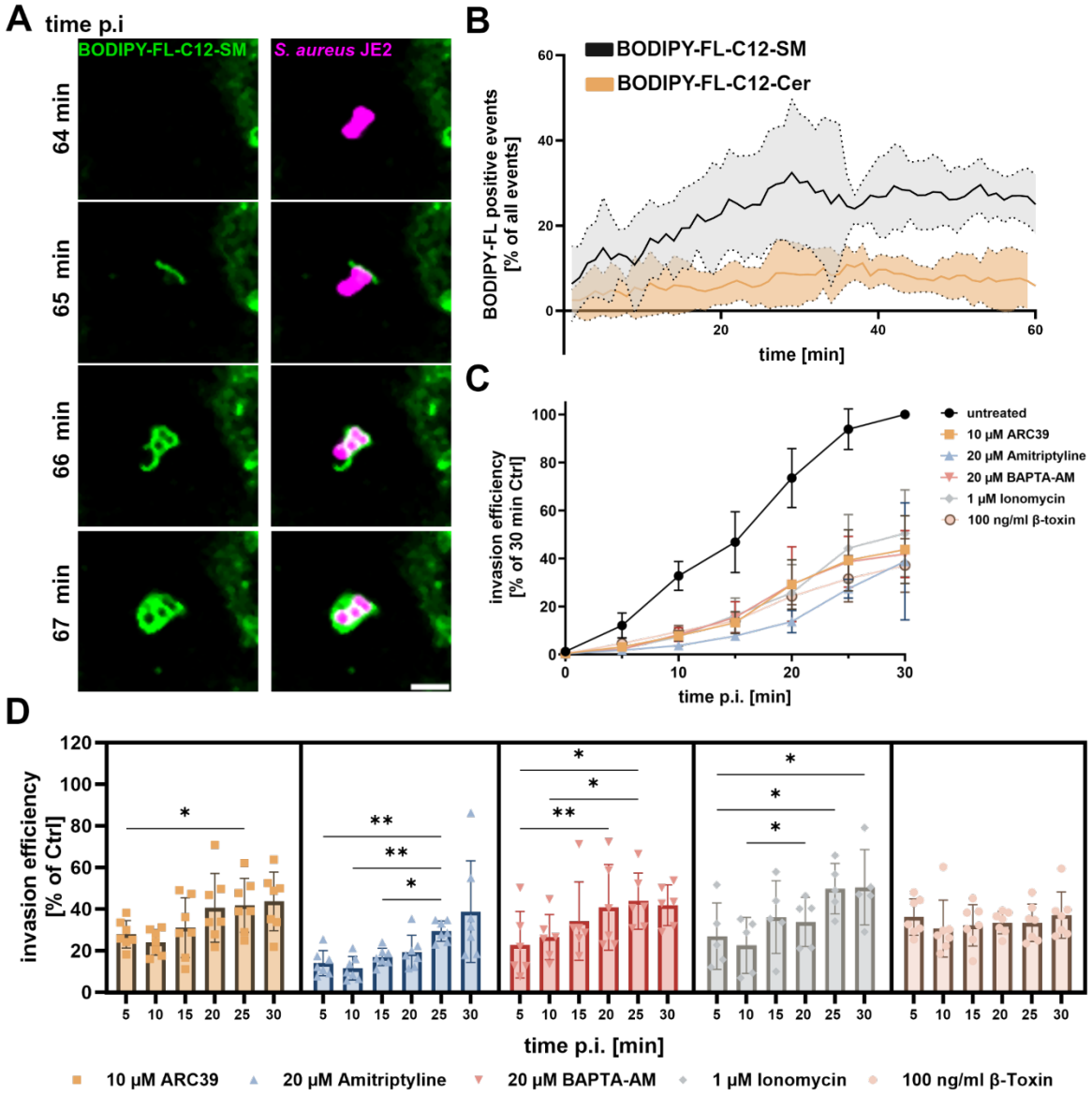

Figure 3 ASM- and Ca^{2+}-dependent uptake is rapid and predominantly mediates invasion early in infection. (A, B) *S. aureus* associates with SM early during invasion. HuLEC were pretreated with BODIPY-FL-C12-SM or BODIPY-FL-C12-ceramide and infected with red-fluorescent *S. aureus*. Scale bar: 5 µm. Infection was monitored by live cell imaging and the proportion of bacteria that associated with the lipid analogs was quantified in each individual frame (SM: n=5, Cer: n=3). **(C, D) ASM and Ca^{2+}-dependent invasion is rapid.** HuLEC were treated with ARC39, amitriptyline, BAPTA-AM, ionomycin, or the bacterial SMase β-toxin. Then, cells were infected with *S. aureus* and the number of invaded bacteria was determined after different time periods. The results were either normalized to the 30 min time point of untreated controls (C) or to the corresponding time points of

the untreated controls (D). (n ≥5). Statistics: Mixed effect analysis and Tukey‘s multiple comparison. Graphs represent means ± SD. *p≤0.05, **p≤0.01, ***p≤0.001, ****p≤0.0001.

The mode of S. aureus invasion affects infection outcome

Next, we tested whether the pathway used for host cell entry also affects the intracellular fate of *S. aureus*. After invasion, the bacteria reside within Rab5-positive early and subsequently, in Rab7-positive late phagoendosomes (39). To trace phagosome maturation, we generated a HeLa cell line stably expressing mCherry-Rab5 as well as YFP-Rab7 and infected with *S. aureus*. We observed that the bacteria transiently associate with Rab5 for a few minutes, before they become positive for Rab7 (**Supp. Video 3**).

We next blocked the ASM-dependent invasion pathway by amitriptyline treatment and infected with *S. aureus* for different time periods. We determined the proportion of bacteria that was associated with Rab5 and/or Rab7 (**Figure 4**, A; see **Supp. Figure 4** for bacteria proportion that associates with Rab7). While ASM inhibition only marginally affected *S. aureus* association with Rab5-positive phagosomes, the proportion of bacteria residing in Rab7-positive vesicles was significantly reduced when compared to the untreated control. This observation was restricted to shorter infection pulses (5-45 min) and was not observed for long infection periods (60 min).

We also observed a reduced proportion of bacteria associated with Rab7-positive membranes after treatment with PCK310 or bacterial SMase (**Supp. Figure 4**, B, C). Forty-five minutes p.i., about half of the bacteria were localized to Rab7-positive vesicles in untreated cells, whereas only ~40% associated with Rab7 upon amitriptyline, PCK310 or β-toxin treatment (**Supp. Figure 4**, C). However, this was not caused by translocation of *S. aureus* to the host cytosol, which was excluded by expressing the fluorescence reporter RFP-CWT (42) in the YFP-Rab7 cell line. Accordingly, RFP-CWT-labelled bacteria in the host cytosol were excluded from the data set [**Supp. Figure 4**, B-D,, (42)]. Hence, ASM-dependently generated phagoendosomes possess different maturation dynamics when compared to phagosomes formed in an ASM-independent fashion.

Next, we measured phagosomal escape while simultaneously detecting SM content of disrupted phagosomal membranes. Therefore, we used a HeLa reporter cell line that cytosolically expresses the phagosomal escape reporter RFP-CWT (42) as well as the SM reporter Lysenin^{W20A}-YFP (82), respectively (**Figure 4**, B). To validate the reporter system, we removed SM from the plasma membrane by β-toxin treatment prior to infection and monitored phagosomal escape by live cell imaging (**Supp. Figure 5**, **Supp. Video 4**). Bacterial translocation into the host cytosol is, again, indicated by recruitment of RFP-CWT. In untreated cells, phagosomal escape was accompanied by recruitment of Lysenin^{W20A}-YFP to vesicular membranes, suggesting that SM located at the luminal leaflet of phagosomes was exposed to the cytosol. By contrast, Lysenin^{W20A}-YFP was not recruited to escape events in β-toxin-treated cells, indicating that the SMase had removed SM from the membranes.

Next, we tested whether internalization of the bacteria via the ASM-dependent pathway would affect phagosomal escape of *S. aureus*. We first confirmed that invasion of *S. aureus* is sensitive to ASM inhibitors and β-toxin treatment, despite reporter gene expression in the cell line (**Supp. Figure 4**, E).

Then reporter cells either were left untreated or were pre-exposed to ASM inhibitors and were infected with *S. aureus* strain JE2. In addition, *S. aureus* Cowan I, a non-cytotoxic strain known to have low escape rates, was used for infection. The proportion of bacteria that escaped from the phagosome (**Figure 4**, C, D) as well as the proportion of escape events, which were additionally positive for cytosolic SM (**Supp. Figure 4**, F) were determined 1.5 h and 3 h p.i. (see also **Supp. Figure 6**, A-D).

Whereas no differences for Lysenin-positive escape events were detected (**Supp. Figure 4**, F), a higher proportion of bacteria escaped from phagosomes on abrogation of ASM activity regardless of the inhibitor used (**Figure 4**, C, D). A similar increase was observed when we blocked lysosomal exocytosis by Vacuolin-1 ((**Figure 4**, E), suggesting that the lack of ASM delivery to the host cell surface during bacterial invasion affects phagosomal escape.

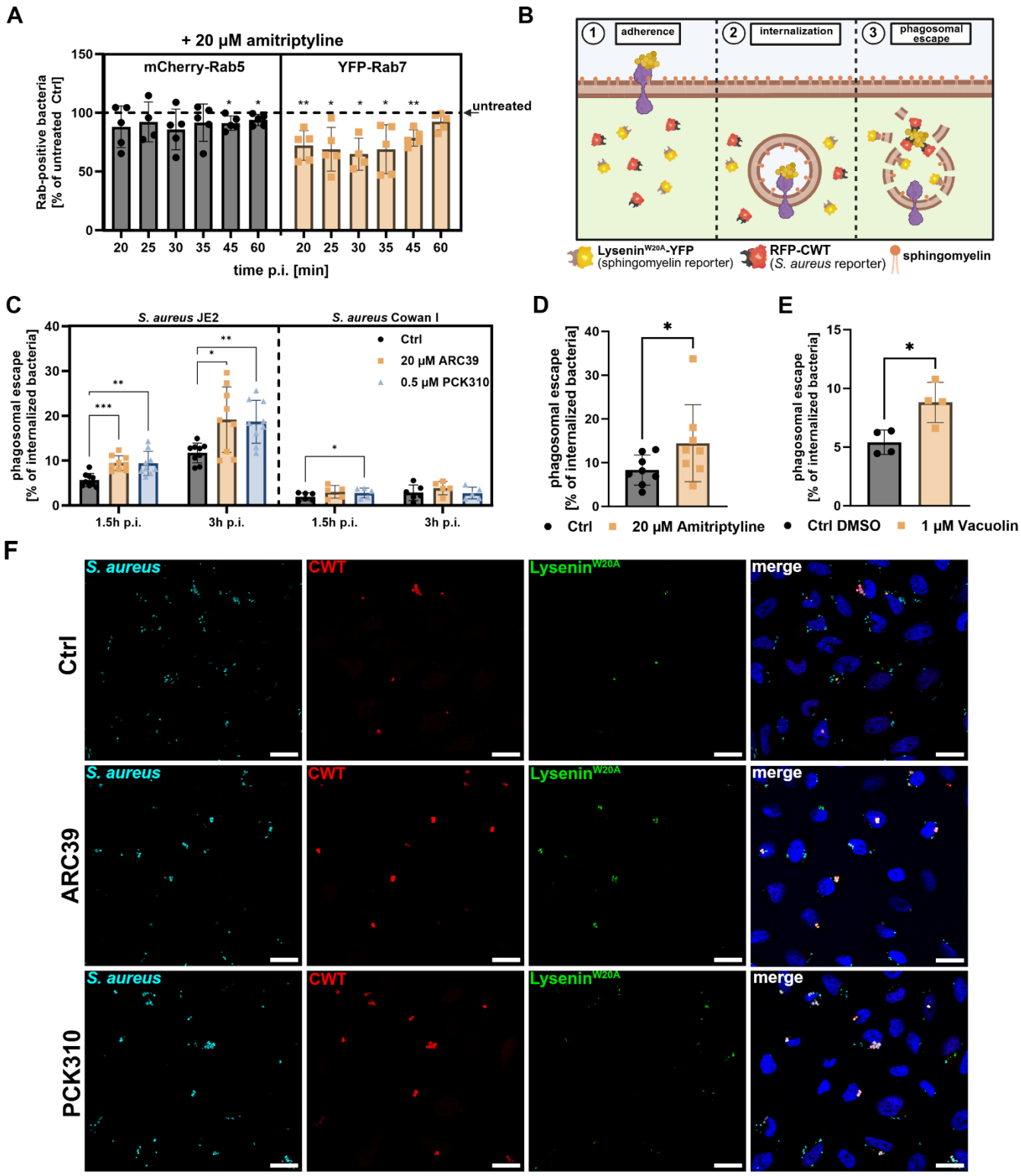

Figure 4 Blocking ASM-dependent invasion affects phagosomal maturation and escape during *S. aureus* infection

(A) Inhibition of ASM delays formation of Rab7-positive phagosomes. HeLa cells expressing mCherry-Rab5 and YFP-Rab7 were either treated with amitriptyline or left untreated. Then, cells were infected with *S. aureus* JE2 for indicated periods. Extracellular bacteria were removed and percentage of intracellular bacteria which associated with Rab5 or Rab7 was determined by CLSM. Results obtained for amitriptyline-treated samples were normalized to untreated controls (n=5). **(B) Detection of phagosomal SM and phagosomal escape by a reporter cell line expressing Lysenin^{W20A} -YFP and RFP-CWT.** After internalization, *S. aureus* resides in a phagosome preventing the recruitment of RFP-CWT to *S. aureus* cell wall and Lysenin^{W20A}-YFP to luminal SM, respectively. When the bacteria lyse the phagosomal membrane, luminal SM gets exposed to the cytosol and attracts

Lysenin^{W20A} -YFP, while RFP-CWT is recruited to the staphylococcal surface. (**C-F) Blocking ASM-dependent internalization affects phagosomal escape.** RFP-CWT and Lysenin^{W20A} -YFP expressing HeLa were treated with PCK310,ARC39 (C, F), amitriptyline (D) or Vacuolin-1 (E) and infected with *S. aureus* strains JE2 or Cowan I. By CLSM, proportions of bacteria that recruited RFP-CWT (phagosomal escape) were determined 3h p.i. if not indicated otherwise (n≥3). **Statistics:** one sample t-test (A), Mixed effects analysis (REML) and Tukey's multiple comparison (C,), paired Student´s t-test (D, E) Graphs represent means ± SD. *p≤0.05, **p≤0.01, ***p≤0.001, ****p≤0.0001.

Since blocking of ASM-dependent uptake reduced invasion efficiency yet increased phagosomal escape rates, we hypothesized that the presence of SM on the plasma membrane affects downstream events during *S. aureus* infection. To address this, we pretreated host cells with the bacterial SMase β-toxin to block SM-dependent invasion (**Figure 5**, A; 2a, 2b) and either infected the cells in presence (**Figure 5, A;** 3a) or after removal of the toxin (3b). β-toxin pretreatment, resulted in enhanced phagosomal escape rates of *S. aureus* JE2, independent of the presence of β-toxin during infection (**Figure 5**, B; 4a, 4b). This was not observed for infections with the Cowan I strain, indicating that removal of SM by β-toxin did not affect general phagosomal membrane stability (**Supp. Figure 4**, G). Moreover, β-toxin treatment strongly reduced recruitment of Lysenin^{W20A}, demonstrating effective removal of SM from membranes by β-toxin (**Figure 5**, C and **Supp. Figure 6**, E-J).

To investigate if removal of SM was important at the cell surface or within the phagosome, we infected the cells with transgenic *S. aureus* JE2 strain either collinearly overexpressing β-toxin and cyan-fluorescent reporter Cerulean or solely expressing Cerulean. We did not observe increased phagosomal escape upon overexpression of β-toxin (**Figure 5**, B; 4c), although Lysenin recruitment to phagosomal membranes was reduced to levels of β-toxin-pretreated samples (**Figure 5**, C). Moreover, we did not detect substantial differences in escape rates of *S. aureus* 6850, a strain naturally producing β-toxin (**Supp. Figure 4**, H), and its isogenic β-toxin mutant. Again, escape of *S. aureus* 6850 was enhanced upon pretreatment with β-toxin (**Supp. Figure 4**, I) accompanied by absence of SM from phagosomal membranes (**Supp. Figure 4**, J).

Phagosomal escape of *S. aureus* thus is independent of SM levels within the infected phagosomes but rather reflects the presence of SM and ASM at the plasma membrane during host cell entry.

We previously showed that *S. aureus* predominantly enters host cells via the rapid ASM- and Ca^{2+}-dependent pathway early upon host cell contact (**Figure 1**, C; **Figure 2**, F; **Figure 3**, D), while other pathways are likely employed later during infection. Consequently, the proportion of pathways (ASM-dependent vs. ASM-independent) that is used for host cell entry relies on the infection time. To demonstrate that phagosomal escape is dependent on the pathway of cell entry, we infected reporter cells with *S. aureus* for either a 10 min ("early invaders") or a 30 min infection pulse (representing "early and late invaders") and at 3h p.i. we determined phagosomal escape rates (**Figure 5**, D) as well as the number of invaded bacteria (**Supp. Figure 4**, K). Independent of the multiplicity of infection (MOI) used, bacteria taken up within the first 10 min demonstrated significantly lower escape rates when compared to bacteria that were cocultured with host cells for 30 min.

This was corroborated by HeLa YFP-CWT infected with *S. aureus* expressing a fluorescent protein (e.g. mRFP) for 30 min ("early and late invaders"). After 20 min, we initiated a second infection pulse for 10 min ("early invaders") with a *S. aureus* strain expressing another fluorescence protein (e.g. Cerulean) and determined phagosomal escape rates of both bacterial recombinants (**Figure 5**, E). Again, early invaders demonstrated lower escape rates when compared to the 30 min control. This was independent of the fluorescent marker expressed by the strain that was used for each infection pulse.

Taken together, we observed higher escape rates 3h p.i., whenever we blocked the rapid ASM-dependent invasion pathways. Consistently, escape rates of bacteria predominantly internalized via the ASM-dependent route ("early invaders") were decreased (**Figure 5**, F). Hence, we concluded that the pathway of host cell entry directly affects phagosomal escape.

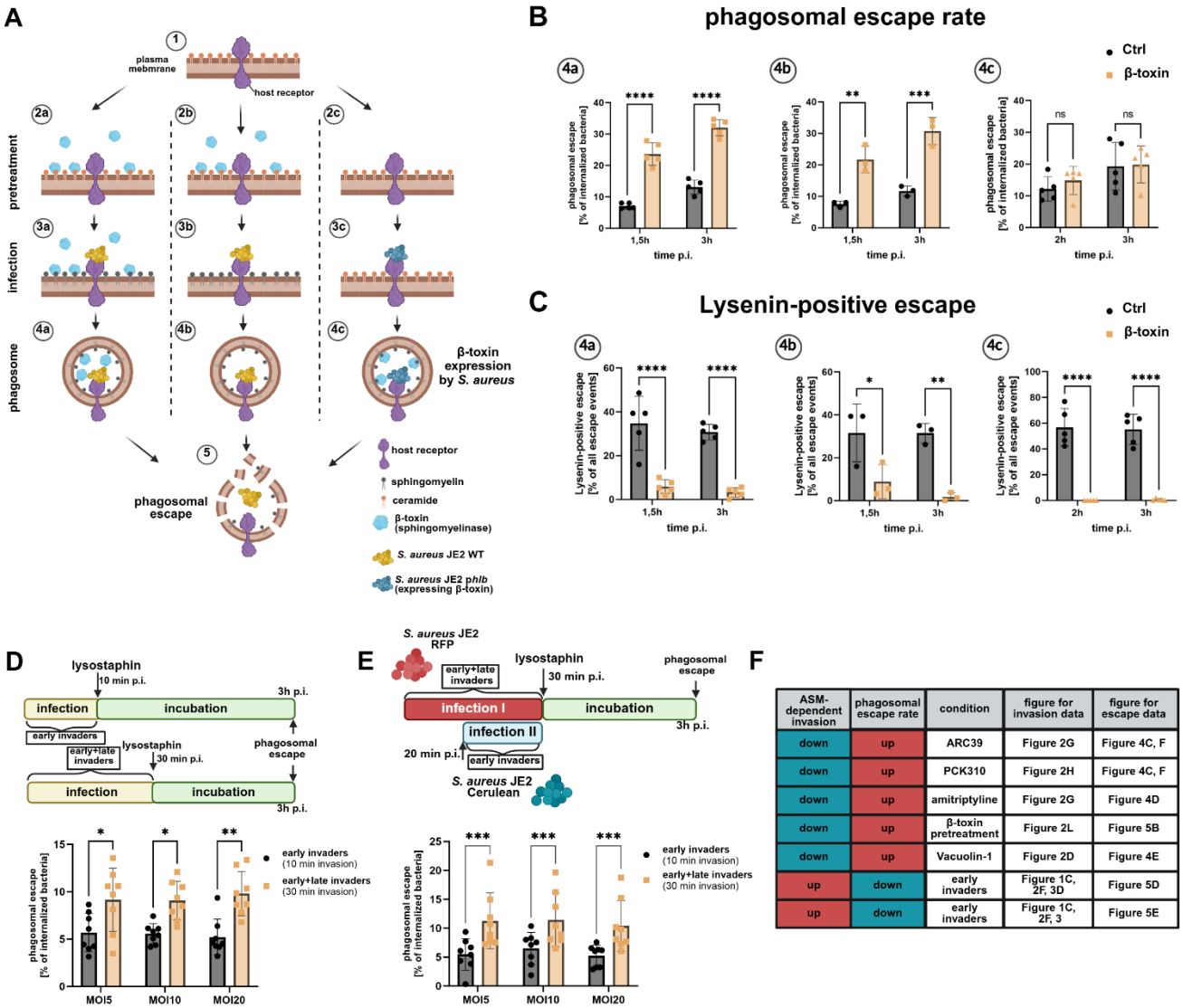

ASM-dependent invasion	phagosomal escape rate	condition	figure for invasion data	figure for escape data
down	up	ARC39	Figure 2G	Figure 4C, F
down	up	PCK310	Figure 2H	Figure 4C, F
down	up	amitriptyline	Figure 2G	Figure 4D
down	up	β-toxin pretreatment	Figure 2L	Figure 5B
down	up	Vacuolin-1	Figure 2D	Figure 4E
up	down	early invaders	Figure 1C, 2F, 3D	Figure 5D
up	down	early invaders	Figure 1C, 2F, 3	Figure 5E

Figure 5 The intracellular fate of *S. aureus* is determined by host cell entry

(A-C) Phagosomal escape depends on presence of plasma membrane SM during invasion, but not presence of SM within phagosomal membranes HeLa RFP-CWT Lysenin^{W20A} -YFP were pretreated with β-toxin to remove surface SM (2a, 2b) or left untreated (2c). Then, cells were infected with *S. aureus* JE2 in presence (3a) or absence (3b) of β-toxin. Untreated samples (3c) were infected with *S. aureus* JE2 harboring a plasmid either encoding β-toxin and the fluorescence protein Cerulean (pCer+*hlb*) or solely Cerulean (pCer). Proportion of bacteria that recruited RFP-CWT (phagosomal escape, B) and the percentage of phagosomal escape events that additionally were positive for Lysenin^{W20A}-YFP (C) were determined at indicated time points p.i. (n=5). **(D, E) Early ASM-dependent invaders possess lower escape rates than late invaders.** HeLa cells expressing RFP-CWT were infected with indicated MOIs of *S. aureus* JE2 either for 10 min (early invaders) or 30 min (early+late invaders). Phagosomal escape rates were determined 3h p.i. (D). HeLa reporter cells expressing YFP-CWT were infected with an MOI=5 of *S. aureus* JE2 expressing a fluorescent protein (e.g. RFP) for 30 min (early+late invaders). After 20 min, the same samples were infected with *S. aureus* JE2 expressing another fluorophore (e.g. Cerulean) for 10 min (early invaders) and phagosomal escape was determined 3 h p.i. (E). **(F) Summary of experiments analyzing the influence of invasion pathway on phagosomal escape.** The measured effects of different conditions on rapid ASM-dependent invasion and accompanied alterations in phagosomal escape rates are summarized. red = increased, blue=decreased. **Statistics:** Two-way ANOVA and Šídák's multiple comparisons test (B-E). Graphs represent means ± SD. *p≤0.05, **p≤0.01, ***p≤0.001, ****p≤0.0001.

We next monitored phagosomal escape over 10 h in cells pretreated with ASM inhibitors (**Figure 6**, A; **Supp. Video 5**; see **Supp. Figure 7**, for absolute bacteria numbers of individual replicates). ASM inhibition enhanced escape rates 3 h p.i. when compared to untreated controls. In contrast, 6 h p.i. escape rates were found decreased upon ASM inhibition.

Taken together, the efficiency of phagosomal escape of *S. aureus* is directly affected by the mode of cell entry, whereby the rapid SM/ASM-dependent pathway results in delayed phagosomal escape, while bacteria that entered host cells ASM-independently escape earlier during infection.

Since translocation to the host cytosol is a prerequisite for *S. aureus* replication in non-professional phagocytes, we recorded intracellular growth of *S. aureus.* In untreated controls replication started about 5 h p.i., and thus shortly after phagosomal escape (3-4 h p.i., **Figure 6**, B). By contrast, we did not observe significant bacterial replication in cells treated with ASM inhibitors (**Figure 6**, B).

We next treated HuLEC with β-toxin, stained the cells with BODIPY-FL-C12-SM and infected the cells with fluorescent *S. aureus*. Live cell imaging demonstrated that most untreated host cells died after 11 h p.i., whereas β-toxin-treated samples showed higher survival rates (**Figure 6**, C; **Supp. Video 6**). This was also observed by cell death assays measuring i) membrane integrity (7-AAD staining, **Figure 6**, D), ii) apoptosis (Annexin V staining, **Figure 6**, E), iii) number of host cells that remained attached to the substratum (**Supp. Figure 8**, A) and iv) host cell lysis by LDH release (**Supp. Figure 8**, B) at 21 h p.i..

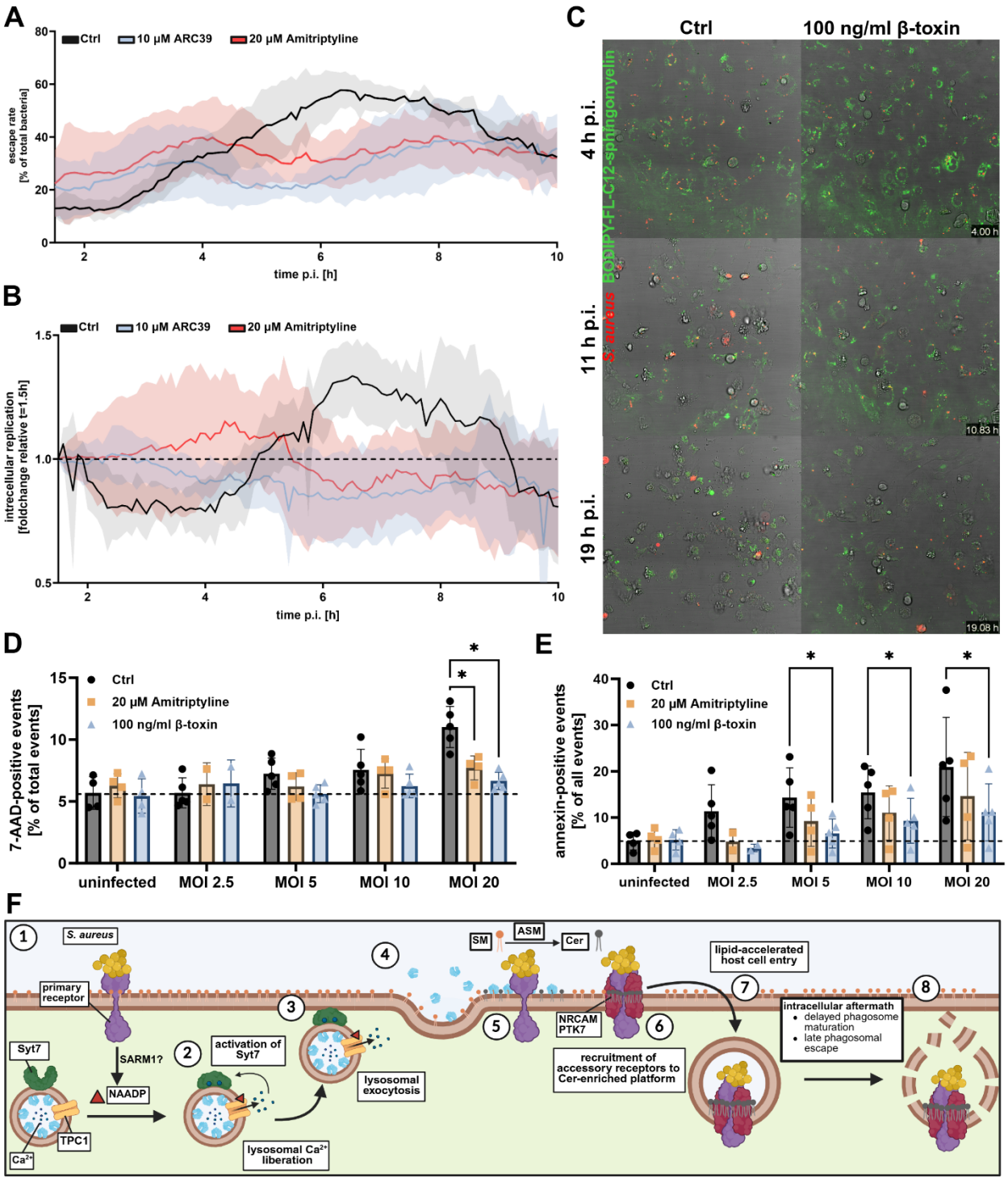

Figure 6 Blocking ASM-dependent internalization affects intracellular replication and host cell survival. **(A, B)** HeLa cells expressing RFP-CWT and Lysenin^{W20A}-YFP were treated with amitriptyline or ARC39 or were left untreated (Ctrl). The cells were subsequently infected with *S. aureus* and infection was monitored for 10 h by CLSM. Proportion of escaped bacteria (A) or the intracellular replication (B) was determined (n= 5). **(C)** HuLEC were stained with BODIPY-FL-C12-SM (green), and were either pretreated with 100 ng/ml of β-toxin or were left untreated. Then, cells were infected with *S. aureus* (red) and infection was monitored by CLSM for 19 h. **(D, E)** HuLEC were treated with amitriptyline or β-toxin and subsequently infected with *S. aureus*. After 21 h, plasma membrane integrity was measured by 7-AAD staining (D), and proportion of apoptotic cells was determined by annexin V staining (E) (n=5). See also **Supp. Figure 8**. (F) Model: *S. aureus* interacts with an unknown primary receptor (1) that triggers production of NAADP, which in turn activates TPC1 to mediate lysosomal Ca^{2+} release and activation of Syt7 (2). Syt7-dependent lysosomal exocytosis (3) leads to release of

503 ASM (4) and production of Cer on the plasma membrane (5) thereby resulting in the recruitment of co-receptors
504 [6,(83)] and rapid internalization of *S. aureus* by host cells (7). Bacteria, which enter the host cells via the rapid
505 pathway, experience a different intracellular fate than bacteria that employed other pathways. **Statistics:** Mixed
506 effects analysis (REML) and Tukey‘s multiple comparison test. Graphs represent mean ± SD. *$p \leq 0.05$.
507
508 **Discussion**
509 ASM has been previously reported to be implicated in the invasion of several viral, bacterial, and
510 eukaryotic pathogens (7, 8, 13-17). However, the dynamics of ASM-mediated host cell entry, the
511 underlying receptors as well as effects on post-invasion events are only poorly understood.
512 We here show that ASM is involved in the uptake of *S. aureus* by certain human cells within minutes
513 after the pathogen contacts the host cell and this pathway is concurrent with ASM-independent uptake
514 pathways. We demonstrate that the infection outcome of bacteria that enter the host cells via this rapid
515 pathway is distinct from other entry mechanisms.
516 We observed a reduction of bacterial invasiveness upon treatment with different ASM inhibitors (**Figure**
517 **2**, G) or removal of the enzyme substrate SM from the plasma membrane (**Figure 2**, L) confirming that
518 ASM activity on the host cell surface is crucial for pathogen internalization. Surprisingly, the uptake of
519 *S. aureus* by ASM K.O. cells was similar to wildtype cells (**Figure 2**, I). However, in ASM K.O.s *S.*
520 *aureus* invasion was only slightly affected by the ASM inhibitor ARC39, while ARC39-treated wildtype
521 cells showed a stronger reduction (**Figure 2**, J). We concluded that reduced invasion in wildtype cells
522 upon ARC39 treatment is mostly due to inhibition of ASM and consistently, the effect of ARC39 is
523 strongly attenuated in ASM K.O.s. Hence, we postulate that other ASM-independent host cell pathways
524 are upregulated in ASM K.O.s, which might be caused by the strongly altered sphingolipid profile
525 detected in ASM K.O.s (**Figure 2**, K). For instance, *S. aureus* internalization by host cells is strongly
526 restricted by caveolin-1, a protein associated with lipid membrane domains (76, 77). Accordingly,
527 alterations in membrane composition might affect distribution of caveolin-1 on the plasma membrane,
528 thereby fostering uptake of *S. aureus*. In consistence, previous studies reported dysfunction of caveolin-
529 1-dependent endocytic processes in ASM-deficient cells (78, 79).
530 Release of ASM is caused by lysosomal exocytosis (6). Conventional methods for detection of
531 lysosomal exocytosis often depend on the usage of anti-LAMP1 antibodies that are added to the cell
532 culture medium for monitoring LAMP1 exposure on the plasma membrane (66). However, most
533 antibodies are non-specifically bound by staphylococcal protein A (84) and hence, these protocols are
534 not compatible with *S. aureus* infection studies. Therefore, we developed a novel approach to measure
535 lysosomal exocytosis via a split luciferase-based assay that demonstrated lysosomal exocytosis during
536 *S. aureus* infection (**Figure 2**, A-C). Consequently, depleting host cells from lysosomes that can undergo
537 Ca^{2+}-dependent exocytosis by ionomycin pretreatment, reduced invasion, even though ionomycin can
538 influence general host cells Ca^{2+} homeostasis (85). Additionally, the lysosomal exocytosis inhibitor
539 Vacuolin-1 resulted in drastically reduced internalization of bacteria (**Figure 2**, D), although the
540 substance is known for side effects such as inhibition of PIKfyve thereby affecting the endo-lysosomal
541 compartment (86). However, we confirmed the role of lysosomal exocytosis for *S. aureus* invasion of
542 host cells by genetic ablation of Syt7, a key protein in lysosomal exocytosis (69).) It remains elusive,
543 which other factors are involved in delivery of lysosomes to and fusion of lysosomes with the plasma
544 membrane. Next to Syt7, there might be other proteins such as Synaptotagmin 1 with overlapping
545 function that could compensate for the absence of Syt7 (87).
546 Elevation of cytosolic Ca^{2+} levels lead to recruitment of lysosomes to the cell surface (67). Whereas
547 most studies implicated Ca^{2+} influx from the extracellular milieu (7, 16), we here demonstrate that *S.*
548 *aureus* mainly triggers lysosomal Ca^{2+} mobilization as was shown by treatment with the inhibitor *trans*-
549 Ned19 as well as a genetic K.O. of the endo-lysosomal Ca^{2+} channel TPC1 (**Figure 1**, B and E; **Supp.**
550 **Figure 1**, C). There are two TPCs (TPC1 and TPC2) that mediate lysosomal Ca^{2+} liberation (88), which
551 have previously been associated with regulation of phagocytic processes (89) and host cell entry of

552 several viruses such as Ebola virus (90), Middle East respiratory syndrome coronavirus [MERS-CoV,
553 (91)] or SARS-CoV-II (92). In line with our study, absence of one of the two TPCs severely interfered
554 with infection (90)(91).
555 TPC-dependent Ca^{2+} liberation was shown to induce exocytosis, for instance, during release of cytolytic
556 granules from T cells (93) or during secretion of insulin (94). Our observations suggest that TPC1 is
557 also involved in exocytosis of lysosomes, since exogenous addition of a bacterial SMase immediately
558 before infection rescued the invasion defect in TPC1 and Syt7 K.O. cells (**Figure 2**, M) indicating that
559 reduced invasion results from a decreased delivery of ASM to the host cell surface. Thus, NAADP-
560 dependent Ca^{2+} liberation from lysosomal stores mediates Syt7-dependent fusion of lysosomes with the
561 plasma membrane resulting in the release of ASM (**Figure 6**, F). While ionomycin treatment led to
562 exocytosis of all "releasable" lysosomes, infection with *S. aureus* led to lysosomal exocytosis of only
563 ~30% of the ionomycin control (**Figure 2**, C), suggesting that *S. aureus* likely triggers local lysosomal
564 exocytosis predominantly at host-bacteria contact sites, whereas ionomycin acts globally on all cells. A
565 similar scenario has been observed for exocytosis of cytolytic granules in T lymphocytes, which differed
566 between TPC/NAADP- and ionomycin-induction (93).
567 The conversion of SM to ceramide by ASM has been associated with the generation of ceramide-
568 enriched platforms. These represent lipid microdomains which facilitate the recruitment of certain
569 protein receptors (95, 96). We previously observed the interaction of *S. aureus* with several host cell
570 surface receptors such as NRCAM or PTK7. The interaction of *S. aureus* with several host receptors
571 was reduced upon blocking ASM-dependent internalization of *S. aureus* (83). It is thus tempting to
572 speculate that accessory receptors identified in this study may be recruited to bacteria-host contact sites
573 to facilitate rapid pathogen internalization.
574 Inhibition of CD38, a known NAADP producer (56, 57), did not influence uptake of staphylococci
575 (**Supp. Figure 1**, H). By contrast, we detected a decreased invasion in cells deficient for the Toll-like
576 receptor adaptor protein SARM1, an alternative NAADP producer [**Figure 1**, D; (59)]. However, the
577 role of SARM1 in lysosomal exocytosis and ASM release requires further investigation. The impact of
578 SARM1 on internalization of *S. aureus* was rather moderate, suggesting the existence of other NAADP-
579 generating enzymes, such as the recently identified NADPH oxidases DUOX1, DUOX2, NOX1 and
580 NOX2(60).
581 One important characteristic of the ASM-dependent internalization pathway is its velocity - taking place
582 within the initial ten minutes of an infection with *S. aureus*, during which treatment with small molecules
583 (**Figure 3**, D), as well as genetic ablation of TPC1 (**Figure 1**, C) and Syt7 (**Figure 2**, F) resulted in
584 reduction of intracellular bacteria. This was accompanied by the quick formation of *S. aureus*-containing
585 phagosomes decorated with fluorescent SM analogs (**Figure 3**, A; **Supp. Figure 3**, **Supp. Video 1**,
586 **Supp. Video 2**).
587 Neither treatment with inhibitors or enzymes nor genetic ablation blocking the rapid internalization
588 pathway abolished the bacterial invasion of host cells completely. This supports our hypothesis that
589 several concomitant host cell entry pathways exist, which is corroborated by a large number of host cell
590 receptors interacting with *S. aureus* (13, 28, 31, 33-38). This pathway exists only in certain host cell
591 types, since among the cell types, as is -for instance- illustrated by our experiments in which
592 internalization of *S. aureus* was only sensitive to ASM inhibition in endothelial (HuLEC and HuVEC)
593 and HeLa cells (**Figure 2**, G). The proportion of bacteria taken up by rapid internalization is dependent
594 on the duration of infection and is higher in early (~50-80% of all internalized bacteria 10 min p.i.)
595 compared to late infection (~15-50% of all internalized bacteria 30 min p.i.).
596 For simplicity we describe the pathway investigated in this study as "rapid" or "ASM-dependent",
597 however a clear cut between this and other pathways cannot be easily delineated. Additionally,
598 internalization factors such as host cell receptors might possess overlapping function and could be
599 involved in several pathways. In this context, ASM might simply accelerate certain internalization
600 pathways, which could also take place in a slower fashion without involvement of ASM.

601 When we blocked the rapid internalization pathway by ASM inhibitors (**Figure 4**, A, C; **Supp. Figure**
602 **4**, B), Vacuolin-1 (**Figure 4**, E, **Supp. Figure 4**) or by removal of surface SM (**Figure 5**, B ; **Supp.**
603 **Figure 4**, B, C), we observed changes in both, maturation of bacteria-containing vesicles and
604 phagosomal escape. A delayed maturation of phagosomes may affect acidification of the vesicles, a
605 property that is sensed by *S. aureus* leading to expression of a different subset of virulence factors (97)
606 and hence may alter intracellular pathogenicity.
607 The bacterial SMase β-toxin originates from *S. aureus*, however, most human pathogenic *S. aureus*
608 strains including JE2, the strain we use in the present study, do not produce β-toxin, due to a genomic
609 integration of a prophage (80). Phagosomal escape of *S. aureus* only was dependent on SM on the plasma
610 membrane during invasion but not on the presence of SM within the phago-endosome (**Figure 5**, A-C;
611 **Supp. Figure 4**, I, J). This not only corroborated that phagosomal escape of clinically relevant *S. aureus*
612 strains is independent of the bacterial SMase β-toxin (42), but also demonstrated that the outcome of
613 phagosomal escape is influenced by processes at the plasma membrane during cell entry.
614 To exclude that inhibitor or bacterial SMase treatment caused changes in phagosomal escape by
615 affecting cellular processes other than bacterial uptake, we infected untreated wildtype cells with *S.*
616 *aureus* for 10 or 30 min, respectively, and monitored phagosomal escape. Bacteria that invaded within
617 the first 10 minutes after contacting host cells ("early invaders") are predominantly ASM-dependent
618 (**Figure 3**) and demonstrated significantly less phagosomal escape (**Figure 5**, G, H). Consistently,
619 blocking the ASM-dependent pathway led to increased proportions of ASM-independent invaders,
620 which in turn resulted in higher escape rates (**Figure 4**, C-E; **Supp. Figure 4**, G). Intracellular *S. aureus*
621 infections thus are directly influenced by the mode of internalization. This ultimately resulted in lower
622 host cytotoxicity (**Figure 6**, C-E; **Supp. Figure 8**) and bacterial replication (**Figure 6**, B) when we
623 blocked the ASM-dependent invasion.
624 An uptake-related intracellular fate has been suggested for *Mycobacterium bovis* (46), *Toxoplasma*
625 *gondii* (48) or *Brucella abortus* (49). However, in these studies the host cells were either depleted from
626 cholesterol, which causes a variety of side effects (47), or internalization was artificially induced by
627 chemicals or ectopic expression of receptors, respectively.
628 Taken together, we here describe a rapid internalization pathway for *S. aureus* into human epithelial and
629 endothelial cells. Bacteria that enter the host cells via this infection route face a distinct intracellular
630 fate. Here we show, to our knowledge, for the first time that host cells within the same population can
631 be invaded by a pathogen via distinct routes and that this results in a differential infection outcome.
632 Rapid internalization may prove beneficial for pathogens in an *in vivo* setting since internalization by
633 host cells shortens the exposure to the innate immune system within a host. Interestingly, the absence of
634 ASM in *Smpd1*$^{-/-}$ mice enhanced the potency of antibiotics to clear *S. aureus* sepsis (98). It is tempting
635 to speculate that reduced host cell invasion in absence of ASM caused a prolonged exposure of the
636 pathogen to antibiotics. Several FIASMAs are already approved drugs (99), and may have future use in
637 infection treatment.
638
639 **Acknowledgements:**

640 This work was supported by the Deutsche Forschungsgemeinschaft (DFG; https://www.dfg.de) within
641 the research training group RTG2581 (M.R., F.S.). C.K. and C.A. are grateful to the DFG AR 376/22-1.
642 M.R. was supported by funds of the Bavarian State Ministry of Science and the Arts and the University
643 of Würzburg to the Graduate School of Life Sciences (GSLS), University of Würzburg. The DFG funded
644 the Leica TCS SP5 CLSM under project code 116162193 and the BD FACSAriaIII cell sorter under
645 project code 206080318.
646 We thank Sibylle Schneider-Schaulies and Thomas Rudel for valuable discussions and critically reading
647 the manuscript, and Nadine Vollmuth as well as Christian Stigloher for scientific advice and intense
648 discussions. We further thank Daniel Herrmann for assistance with HPLC-MS/MS measurements of

sphingolipids. We are indebted to Kathrin Stelzner for conducting FACS of cell lines and generation of *S. aureus* strains. TPC1/2 double-knock out HeLa cells were kindly provided by Norbert Klugbauer (Freiburg, Germany). pmRFP-LC3 was a gift from Tamotsu Yoshimori (Addgene plasmid # 21075; http://n2t.net/addgene:21075; RRID:Addgene_21075, (100)). pLVTHM (101), pMD2.G and psPAX2 (unpublished) were a gift from Didier Trono (Addgene plasmids # 12247, 12259 and 12260, respectively). pLX304-Flag-APEX2-NES was a gift from Alice Ting (Addgene plasmid # 92158, (102)) and pSpCas9(BB)-p2A-GFP (PX458) (74) was a gift from Feng Zhang (Addgene plasmid # 48138; http://n2t.net/addgene:48138). Figures were created in BioRender.

Author Contributions:

M.R., M.F. conceptualized the work, designed the methodology and wrote the original draft manuscript. M.F., B.K. acquired funding. M.R. F.S., K.U., M.P., A.M., N.K., J.W., A.I., C.K., K.P., F. Schu performed the experiments; M.R., M.F. supervised the experiments. M.R., C.A., M.F. analyzed the data; all authors edited and revised the manuscript.

Declaration of interests.

Patentability of PCK310 is currently evaluated by C.K. and C.A.

Materials and Methods

Table 1 Oligonucleotides used in this study

Purpose	Name	sequence (5´→ 3´)
Gene deletion	Syt7-sgRNA2 rv	AAACATGACGTCATTGCGGCTGAG
	Syt7-sgRNA2 fw	CACCCTCAGCCGCAATGACGTCAT
	Syt7-sgRNA1 rv	AAACCACGATGAGTCCGACCGCCG
	Syt7-sgRNA1 fw	CACCCGGCGGTCGGACTCATCGTG
	TPCN1-sgRNA2 rv	AAACAGGACGGCGCTCCTCATCTT
	TPCN1-sgRNA2 fw	CACCAAGATGAGGAGCGCCGTCCT
	TPCN1-sgRNA1 rv	AAACTTCAGACCCCGTAAGTAATC
	TPCN1-sgRNA1 fw	CACCGATTACTTACGGGGTCTGAA
	SARM1-sgRNA1 rv	AAACTAGAGTCGAGCAACGGCACG
	SARM1-sgRNA1 fw	CACCCGTGCCGTTGCTCGACTCTA
	SARM1-sgRN2 rv	AAACGCACGTAGAATAGTTGGCGA
	SARM1-sgRNA2 fw	CACCTCGCCAACTATTCTACGTGC
	SMPD1-sgRNA1 fw	CACCAGCCAGGGTGTTCTCATACC
	SMPD1-sgRNA1 rv	AAACGGTATGAGAACACCCTGGCT
	SMPD1-sgRNA2 fw	CACCGTTCTTTGGCCACACTCATG
	SMPD1-sgRNA2 rv	AAACCATGAGTGTGGCCAAAGAAC
Cloning	MP-mRFP-f	GAGACTAGCCTCGAGGTTTAAACCACCATGGCCTCCTCCGAGGACGTC
	euk_mRFP-r	GGAATGCCCGGGCGCGCCGGTGGAGTGGCGGC
	infus-CWT-f	ACCGGCGCGCCCGGGCATTCCACGCCCAATACAGGTTGG
	infus-CWT-r	GAGGTTGATTATCATATGACTAGTTCACTTTATAGTTCCCCAAAG
	eYFP-rev	CTTGTTGATGGGCTCGAGCCCTTGTACAGCTCGTCCATGCCGAG
	Pm-eYFP-inf	GACTAGCCTCGAGGTTTAAACCACCATGGTGAGCAAGGGCGAGGAG
	hLysenin-infus-r	GAGGTTGATTATCATATGACTAGTTCAGCCCACCACCTCCAG
	InfReamp-f	GGCTCGAGCCCATCAACAAG
	cYFP-f	ATGGTGAGCAAGGGCGAGGAGCTG
	his1-Flag-f	CATCATCATCATCACGGAGCGGACTACAAGGATGACGACGATAAGG
	his2-Inf-f	GACTAGCCTCGAGGTTTAAACCACCATGGCACATCATCATCATCATCA CGGAGCG
	Apex-YFP-infus-r	CGCCCTTGCTCACCATCTCGAGCCGTCCAGGGTCAGGCGCTCC
	Lamp1-as	GATAGTCTGGTAGCCTGCGTGACTCC
	EF1a_fwd	TCAAGCCTCAGACAGTGGTTC
	LV-WPRE-seq	GTATCCACATAGCGTAAAAGGAGC
	IRES-eYFP-rev	GCCCTTGCTCACCATGGTTGTGGCGCGCCATTATCATCGTGTTTTTC
	LampSP-Hibit-r	GCTAATCTTCTTGAACAGCCGCCAGCCGCTCACTGCTGACGCACAATG CATGAGGC
	Inf-Hibit-LAMP-f	GTTCAAGAAGATTAGCGCAATGTTTATGGTGAAAAATGGC
	Lamp-IRES-f	GGCTACCAGACTATCTAATGAACTAGGGGTAAATTCCGCC
	LgBit-LVPme-fwd	GAGACTAGCCTCGAGGTTTAAACCACCATGGTCTTCACACTCGAAGAT TTCG
	LgBit-LVSpe-rev	GAGGTTGATTATCATATGACTAGTTTAACTGTTGATGGTTACTCGG
	PmeInfus-SPLamp-fwd	GAGACTAGCCTCGAGGTTTAAACCACCATGGCGGCCCCCGGCAGCGC
	LV-Spe-rev	GAGGTTGATTATCATATGACTAG
	cYFP-f	ATGGTGAGCAAGGGCGAGGAGCTG
	Lamp1-p2a-f	GGCTACCAGACTATCGGCAGTGGAGAGGGCAGAGGAAG
	p2a-eYFP-r	CTCGCCCTTGCTCACTGGGCCAGGATTCTCCTC

668 **Cell culture**

669 HeLa (ATCC CCL-2™), 16HBE14o- (kindly provided by Prof. Jan-Peter Hildebrandt, University of
670 Greifswald) and EA.hy 926 (103) were cultivated in RPMI+GlutaMAX™ medium (Gibco™, Cat. No.
671 72400054) supplemented with 10% (v/v) heat-inactivated (56°C at 30 min) fetal bovine serum (FBS,
672 Sigma Aldrich, Cat. No. F7524) and 1 mM sodium pyruvate (Gibco™, Cat.No. 11360088).
673 HuLEC-5a (ATCC CRL-3244™) and HuVEC (Gibco™, Cat. No.C01510C) were cultured in
674 MCDB131 medium (Gibco™, Cat. No. 10372019) supplemented with microvascular growth
675 supplement (Gibco™, Cat. No. S00525), 2 mM GlutaMAX™ (Gibco™, 35050061), 5 % (v/v) heat-
676 inactivated (56°C at 30 min) FBS, 2.76 µM hydrocortisone (Sigma Aldrich, Cat. No. H0888), 0.01 ng/ml
677 human epidermal growth factor (Pep Rotech, AF-100-15) and 1x Penicillin-Streptomycin (Gibco™, Cat.
678 No. 15140122).
679 HeLa
680 HuLEC and HuVEC were detached by StemPro™ Accutase™ (Gibco™, Cat. No. A1110501) and
681 seeded at the indicated density two days prior to the experiment, whereas HeLa, 16HBE14o- and EA.hy
682 926 were detached with TrypLE™ (Gibco™, Cat. No. 12604013) and seeded one day prior to the
683 experiment.
684 **Generation of HeLa KO cell lines**
685 Generation of K.O. cell lines is based on a previous protocol (74). sgRNAs (**Table 1**) were designed
686 with the CHOPCHOP online tool (chopchop.cbu.uib.no) and synthesized as primer pairs (Sigma
687 Aldrich). After phosphorylation with T4 nucleotide kinase (ThermoFisher, Cat. No. ER0031), the
688 sgRNAs were cloned into the BbsI sites of pSpCas9(BB)-p2A-GFP (AddGene #48138, (74)) via forced
689 ligation by BbsI (ThermoFisher, Cat. No. ER1012) and T4 Nulceotide ligase (ThermoFisher, Cat. No.
690 EL0011). The constructs were then transformed in *E. coli* DH5α (ThermoFisher, Cat. No EC0112) and
691 subsequently sequence verified.
692 HeLa cells were transfected with 1 µg each of two distinct sgRNA constructs using JetPrime (Polyplus)
693 following the manufacturer's instructions. After 36-48h, cells were sorted for strong GFP expression in
694 a FACS Aria III (BD Bioscience).To isolate ASM K.O. cell lines, we included a second sorting step.
695 Therefore, the cells were incubated with 10 µM FRET probe (73) for 2 h at 37°C/5% CO_2 and sorted
696 for cells negative in FITC emission, which correlates with the cellular ASM activity. The resulting cell
697 pools were cultivated and tested for loss of expression of the respective sgRNA target by Western
698 Blotting or ASM activity assays.
699 The following antibodies were used: mouse anti-PTK7 monoclonal IgG1 (bio-techne, Cat. No.
700 MAB4499) with a horse radish peroxidase (HRP)-conjugated anti-mouse antibody (SantaCruz, Cat. No.
701 sc-516102) and rabbit anti-TPC1 polyclonal (Thermo Fisher, Cat. No. PA5-41048) or rabbit anti-
702 SARM1 monoclonal antibody (Cell Signaling Technology, Cat. No. 13022) with an HRP-conjugated
703 anti-rabbit antibody (Biozol, Cat. No. 111-035-144).
704

705 **Generation of reporter constructs**
706 *pLV-mRFP-CWT.* mRFP and the cell wall-targeting domain of lysostaphin CWT were amplified using
707 primers MP-mRFP-f and euk_mRFP-r, as well as infus-CWT-f and infus-CWT-r, respectively. As PCR
708 templates we used pmRFP-LC3 (PMID 17534139) and pLV-YFP-CWT (104). The resulting plasmid
709 was termed pLV-mRFP-CWT. The PCR products were subsequently cloned into pLVTHM (101)
710 restricted with PmeI and SpeI by InFusion cloning following the manufacturer's recommendations.
711
712 *pLV-YFP-Lysenin.* The sequence of the sphingomyelin-binding but not pore-forming earthworm toxin
713 mutant Lysenin^{W20A} (82) was synthesized by GeneArt (ThermoFisher) adapted to human codon usage
714 and with a 5' flanking region encoding a glycine-rich linker sequence. The synthesized fragment served
715 as template for subsequent PCRs.

716 Lysenin^{W20} was amplified using oligonucleotides InfReamp-f and hLysenin-infus-r (**Table 1**).
717 YFP was amplified with Pm-eYFP-inf and eYFP-rev from template pLVTHM-YFP-CWT (104). Both
718 PCR products were joined with pLVTHM vector restricted with PmeI and SpeI by InFusion cloning
719 following the manuacturer's recommendations, thereby creating pLV-YFP-Lysenin.
720
721 Constructs were transformed into *E. coli* DH5α and sequences were validated. Plasmid preparations
722 were performed using standard laboratory procedures. VSV-G-pseudotyped Lentiviral particles were
723 generated by transfecting with each lentiviral vector as well as the plasmids pMD2.G (VSV G) and
724 psPAX2 following the protocol of (101) and target cells were transduced as described previously (104).
725
726 **Bacteria culture**
727 *S. aureus* liquid cultures were either grown in 37 g/L brain heart infusion (BHI) medium (Thermo Fisher,
728 Cat. No. 237300) or in 30 g/l TSB medium (Sigma Aldrich, Cat. No. T8907). *E. coli* liquid cultures
729 were grown in LB medium [10 g/l tryptone/peptone (Roth, Cat. No. 8952.4,) 5g/l yeast extract (Roth,
730 Cat. No 2363.2), 10 g/l NaCl (Sigma Aldrich, Cat. No. S5886)].
731 For agar plates, 15 g/L agar (Otto Norwald, Cat. No. 257353), was added to either TSB (*S. aureus*) or
732 LB (E. coli).
733 Media and plates were supplemented with appropriate antibiotics [5 µg/ml erythromycin (Sigma
734 Aldrich, Cat. No. E5389), 10 µg/ml chloramphenicol (Roth, Cat. No. 3886.2), 100 ng/ml Carbenicillin
735 (Roth, Cat. No. 6344.2)].
736 Strains used in this study are listed in **Table 2**.
737

738 **Table 2 Bacterial Strains used in this study**

Strain	Remarks	Source
S. aureus 6850		(105)
S. aureus 6850 Δ*hlb*	deficient in β-toxin production	(42)
S. aureus Cowan I	NCTC 8530, isolated from septic arthritis, agr dysfunction, low expression of toxins and proteases	ATCC 12598
S. aureus JE2	MRSA, USA300	(106)
S. aureus JE2 Δ*hla*	deficient in α-toxin production	(107)
S. aureus JE2 Δ*hlb*	deficient in β-toxin production	(11)
S. aureus JE2 SarAP1 Cerulean	Constitutive expression of the fluorescence protein Cerulean	This work
S. aureus JE2 SarAP1 mRFP	Constitutive expression of the fluorescence protein mRFP	(45)
S. aureus JE2 p*Cer*	Anhydrous tetracycline (AHT) inducible expression of Cerulean, construct published in (108) and was transduced into *S. aureus* JE2	This work
S. aureus JE2 p*Cer+hlb*	Anhydrous tetracycline (AHT) inducible expression of Cerulean and β-toxin, construct published in (108) and was transduced into *S. aureus* JE2	This work
S. aureus Cowan I *SarAP1 Cerulean*	Constitutive expression of the fluorescence protein Cerulean	This work
S. aureus 6850 SarAP1 Cerulean	Constitutive expression of the fluorescence protein Cerulean	(45)
S. aureus 6850 Δ*hlb* SarAP1 Cerulean	Constitutive expression of the fluorescence protein Cerulean	This work

739
740
741 ***S. aureus* growth curves**
742 *S. aureus* overnight cultures were grown in BHI medium, and 1 ml was centrifuged at 14,000 for 1 min.
743 Bacteria were washed thrice with DPBS and either resuspended in BHI (for amitriptyline and ARC39
744 treatment) or infection medium [MCDB131 medium (Gibco™, Cat. No. 10372019) complemented with
745 2 mM GlutaMAX™ (Gibco™, 35050061) and 10 % (v/v) heat-inactivated (56°C at 30 min) FBS, for
746 ionomycin treatment). Bacteria suspensions were diluted to OD_{600}=0.1 in the respective medium. Then,
747 400 µL per well of the suspension as well as respective blanks were transferred into a 48 well plate and
748 OD_{600} was determined every 16 min in Tecan mPlex200 microplate reader.
749
750 ***S. aureus* infections**
751 Host cells were seeded in 6 well plates ($2x10^5$ cells per well), 12 well plates ($1x10^5$ cells per well) or 24
752 well plates ($0.5x10^5$ cell per well) either one day (HeLa, EA.hy 926, 16HBE14o$^-$) or two days (HuLEC,
753 HuVEC) prior to the experiment. Host cells were washed thrice with DPBS and infection medium or
754 Ca^{2+}-free infection medium [DMEM w/o calcium (Gibco™, Cat. No. 21068028) complemented with
755 10 % (v/v) heat-inactivated (56°C at 30 min) FBS and 200 µM BAPTA (Merck Millipore, 196418)]
756 with or without 1.8 mM $CaCl_2$ (Roth, Cat. No. 5239.1) was added. If indicated, cells were pretreated
757 with compounds prior to infection (for details about treatments see **Table 1**). For experiments involving
758 blocking of receptors by antibodies, respective solvent controls were implemented (final concentrations
759 in infection medium: 0.002% (w/v) NaN_3 (Sigma Aldrich, Cat. No. S2002) 5% glycerol (Roth, Cat. No
760 3783.2) in 10% DPBS for 30 ng/ml anti-NRCAM antibody as well as well as 0.01 % (w/v) NaN_3 for
761 50 ng/ml anti-CD73 and 50 ng/ml anti-MELTF antibodies.
762
763 **Table 3 Host cell treatment with various compounds**

compound	Supplier/Cat.No.	preincubation time	removal prior to infection?
2-APB (2-Aminoethoxydiphenylborate)	Sigma Aldrich/ D9754	75 min	removed prior to infection
8-Bromo-cADPR (8-Bromo-cyclic ADP ribose)	Biolog/065-005	75 min	present during infection
amitriptyline	Sigma Aldrich/ A8404	75 min	present during infection
ARC39	(71)	18 h, add fresh inhibitor for another 4h or as indicated	present during infection
BAPTA-AM	Merck Millipore/ 196419; (51)	25 min	removed prior to infection
BODIPY-FL™-C12-Ceramide	Santa Cruz/ sc-503923	90 min	present during infection
BODIPY-FL™-C12-Sphingomyelin	ThermoFisher/D7711	90 min	present during infection
CD38i/78c	Sigma Aldrich/ 5387630001	75 min	present during infection
Ionomycin	Sigma Aldrich/ I0634	75 min	present during infection

PCK310	To be published elsewhere, patent pending	4h or as indicated	present during infection
trans-Ned19	Sigma Aldrich/ SML2830; (55)	75 min	present during infection
Vacuolin-1	Biozol/ MCE-HY-118630	75 min	present during infection
β-toxin	Sigma Aldrich/ S8633	75 min	removed prior to infection if not indicated otherwise

764
765 An *S. aureus* overnight culture grown in BHI containing the appropriate antibiotics was diluted to an
766 OD_{600}=0.4 in the same medium. When inducible expression of genes was required for the strains *S.*
767 *aureus* JE2 p*Cer* and *S. aureus* JE2 p*Cer+hlb,* 200 ng/ml anhydrous tetracycline (AHT, AcrosOrganics,
768 233131000) was added. The culture was grown to an OD_{600}= 0.6-1.0 and 1 ml bacterial suspension was
769 harvested by centrifugation and washed twice with Dulbecco's Phosphate Buffered Saline (DPBS,
770 Gibco^{TM}, Cat. No 14190169). The bacteria were resuspended in infection medium (or Ca^{2+}-free infection
771 medium when infection was performed in absence of extracellular Ca^{2+}). The number of bacteria per ml
772 in the suspension was determined with a Thoma counting chamber and the MOI was determined. If not
773 indicated otherwise, an MOI=10 was used for infections.
774 The infection was synchronized by centrifugation 800xg/8 min/RT (end of the centrifugation: t=0). To
775 determine bacterial invasion, the infection was stopped after 30 min (unless indicated otherwise) by
776 removing extracellular bacteria with 20 µg/ml Lysostaphin (AMBI, Cat. No. AMBICINL) in infection
777 medium for 30 min. Then, host cells were washed thrice with DPBS, lysed by addition of 1 ml/well (12
778 well plate) or 0.5 ml/well (24 well plate) Millipore water and the number of bacteria in lysates was
779 determined by plating serial dilutions (10^{-1}, 10^{-2}, 10^{-3}) on TSB agar plates. Plates were incubated
780 overnight at 37 °C and colony forming units (CFU) were enumerated. To determine invasion efficiency,
781 the number of bacteria determined in tested samples were normalized to untreated controls (set to 100%).
782 For measuring invasion dynamics, the number of bacteria was either normalized to the 30 min time point
783 of untreated controls or to the corresponding time points of untreated controls.
784 If later time points in infection were investigated, infection medium containing 2 µg/ml Lysostaphin
785 was added to the cells until the indicated time.
786 For testing bacterial susceptibility to inhibitors ("survival") or adherence, Lysostaphin treatment was
787 omitted, and host cells were immediately lysed by addition of Millipore water or washed five times with
788 DPBS and subsequently lysed with Millipore water, respectively. The number of bacteria in lysates was
789 determined by CFU counting (dilutions 10^{-2}, 10^{-3}, 10^{-4}) on TSB agar plates.
790
791 **Phagosomal escape assays**
792 For phagosomal escape assays with amitriptyline, ARC39, PCK310 and β-toxin, HeLa cells expressing
793 RFP-CWT and Lysenin^{W20A}-YFP were infected with the indicated *S. aureus* strain as described in the
794 previous paragraph. Infections with *S. aureus* JE2 p*Cer* and *S. aureus* JE2 p*Cer+hlb* were carried out in
795 presence of 200 ng/ml AHT.
796 For phagosomal escape assays, HeLa cells expressing RFP-CWT and Lysenin^{W20A}-YFP were infected
797 for 10 min (early invaders) or 30 min (early and late invaders) at the indicated MOIs.
798 For the phagosomal escape assays with two *S. aureus* JE2 strains expressing different fluorescence
799 proteins, HeLa cells expressing YFP-CWT were infected with an MOI=5 of an initial *S. aureus* JE2
800 strain (*S. aureus* JE2 SarAP1 Cerulean or *S. aureus* JE2 SarAP1 mRFP). After 12 min of infection, a
801 second infection pulse was initiated by adding the second *S. aureus* JE2 strain (expressing the

802 complementary fluorescence protein, *S. aureus* JE2 SarAP1 mRFP or *S. aureus* JE2 SarAP1 Cerulean,
803 respectively) and centrifuging the bacteria on the host cells. To exclude that the type of fluorescence
804 protein expressed by the *S. aureus* strains contributes to the experimental outcome, either strain was
805 used for the first and second infection pulse (each combination: n=4).
806
807 **Phagosomal maturation assays**
808 To monitor phagosomal maturation, HeLa cells expressing mCherry-Rab5 and YFP-Rab7 or YFP-Rab7
809 and RFP-CWT were infected with *S. aureus* JE2 SarAP1 Cerulean.
810 After 3 h p.i. (unless indicated otherwise), cells were washed thrice with DPBS and fixed with 0.2%
811 glutaraldehyde (Sigma Aldrich, Cat. No. 10333) / 4% paraformaldehyde in PBS (Morphisto, Cat. No
812 11762.01000) for 30 min at RT. Then, cells were washed thrice with DPBS, stained with 5µg/ml Hoechst
813 34580 (Thermo Fisher, Cat. No. H21486) and mounted in Mowiol [24g glycerol (Roth, Cat. No. 3783.2),
814 9.6 g Mowiol®4-88 (Roth, Cat. No 0713.2), 48 ml 0.2 M TRIS-HCl pH 8.5 (Sigma Aldrich, Cat. No
815 T1503), 24 ml Millipore water].
816 Samples were imaged with a Leica TCS SP5 confocal microscope (Wetzlar, Germany; Software Leica
817 LAS AF Version 2.7.3.9723) with a 40x immersion oil objective (NA1.3) and a resolution of 1024x1024
818 pixels [Cerulean (Ex. 458 nm/Em. 460-520), YFP (Ex. 514 nm/Em. 520-570nm), mRFP/mCherry (Ex.
819 561 nm/Em.571-635nm) and Hoechst 34580 (Ex. 405 nm/Em.410-460nm). At least 10 fields of view
820 per samples were recorded.
821 Image analysis was performed in Fiji (109) using a previously described macro (108) that identifies
822 and extracts individual bacteria from images as regions of interest (ROIs, see **Supp. Figure 6**).
823 Subsequently, fluorescent intensity in every channel is measured to determine recruitment of
824 fluorescence reporters to the bacteria. Results were exported as text files and proportion of bacteria that
825 recruited individual reporters was determined with the Flowing 2 software (Turku Bioscience Center).
826 Phagosomal escape rates were determined as the proportion of CWT-positive bacteria of the total
827 number of intracellular bacteria. Similarly, the proportion of Lysenin^{W20A}-positive escape events, the
828 ratio of Lysenin^{W20A}-/CWT-positive events and all CWT-positive events was calculated.
829 To measure the proportion of bacteria that were associated with Rab5 and/or Rab7, the proportion of
830 Rab5- and/or Rab7-positive membranes around bacteria of all intracellular bacteria was determined. For
831 experiments obtained with HeLa cells expressing YFP-Rab7 and RFP-CWT, bacteria that acquired RFP-
832 CWT were removed from the dataset. Subsequently, the proportion of Rab7-positive bacteria in relation
833 to all CWT-negative intracellular bacteria was determined.
834
835 **Live cell imaging**
836 The indicated host cells were seeded one (HeLa) or two days (HuLEC) prior to the experiments in µ-
837 slide 8 well live cell chambers (ibidi, Cat. No 80826-90) with a density of 0.375×10^5 cells per well.
838 For monitoring host cell entry, cells were washed thrice with DPBS and were then, incubated for 90 min
839 in infection medium with 1 µM BODIPY-FL-C_{12}-sphingomyelin (Thermo Fisher Cat. No. D7711), 10
840 µM BODIPY-FL-C_{12}-ceramide (Santa Cruz, Cat.No. sc-503923) or 10 µM visible-range FRET probe
841 (73). Pretreatment with the FRET probe was performed in infection medium containing 1 % (v/v) FBS.
842 Then, cells were washed thrice with DPBS and imaging medium [RPMI 1640 w/o phenol red (Gibco™,
843 Cat. No. 11835030) containing 10% (v/v) heat-inactivated (56°C/30 min) FBS (Sigma Aldrich, Cat. No.
844 F7524) and 30 mM HEPES (Gibco™, Cat.No. 15630080)] applied. Samples stained with the FRET
845 probe were imaged in imaging medium containing 1% FBS and in presence of 10 µM FRET probe.
846 Samples were infected with *S. aureus* JE2 SarAP1 Cerulean (FRET probe samples) or *S. aureus* JE2
847 SarAP1 mRFP (BODIPY-FL-C12-sphingomylein/-ceramide) at an MOI=50 without synchronization
848 by centrifugation. Infection was monitored with a Leica TCS SP5 confocal microscope (Wetzlar,
849 Germany) in intervals of 1 min by recording BODIPY-FL (Ex. 496 nm/Em. 500-535 nm), mRFP (Ex.
850 561 nm/Em.571) FITC (Ex. 488 nm/Em. 500-560), Cerulean (Ex. 458 nm/Em. 460-520), BODIPY-TR

851 (Ex. 594 nm/Em. 610-680) and FRET (Ex.488 nm/ Em:610-680) channels. Cells were recorded with a
852 40x immersion oil objective and a resolution of 2048x2048 pixels. For samples stained with the FRET
853 probe, 20 µg/ml Lysostaphin was added 40 min p.i. to remove extracellular bacteria.
854 For quantification of bacteria that associate with BODIPY-FL-C_{12}-sphingomyelin/-ceramide, individual
855 bacteria in single frames were identified, extracted as ROIs and BODIPY-FL fluorescence in ROIs was
856 measured in Fiji (109) as described before for phagosomal escape assays. Results were extracted as text
857 files and the proportion of bacteria associating with BODIPY-FL was determined with Flowing2 (Turku
858 Bioscience Center).
859 For monitoring intracellular *S. aureus* infection, host cells were pretreated and infected with
860 *S. aureus* JE2 SarAP1 Cerulean (HeLa RFP-CWT/Lysenin^{W20A}-YFP) or *S. aureus* JE2 SarAP1 mRFP
861 (HuLEC) as described in "*S. aureus* infection". HuLEC additionally were treated with 1 µM BODIPY-
862 FL-C_{12}-sphingomyelin in infection medium for 90 min and washed thrice with DPBS before the
863 indicated treatment was applied. After extracellular bacteria were removed with 20 µg/ml lysostaphin
864 for 30 min, imaging medium containing 2 µg/ml lysostaphin was applied and infections were monitored
865 in intervals of 5 min (HeLa RFP-CWT) or 20 min (HuLEC). Phagosomal escape was evaluated in Fiji
866 as described above. To determine intracellular replication, the number of bacteria was determined for
867 each individual frame as described before (108). The number of bacteria at each time point was then
868 normalized to the number of bacteria detected in the first frame to calculate the relative replication.
869
870
871
872 **ASM and NSM activity assays**
873 Thin layer chromatography (TLC)-based ASM/NSM activity assays were adapted from previously
874 published protocols (72). To determine cellular ASM activity, the indicated cell lines were seeded in 24
875 well plates with a density of $1x10^5$ cell per well one day (HeLa, EA.hy 926, 16HBE14o$^-$) or two days
876 (HuLEC, HuVEC) prior to the experiment. Cells were either treated with 20 µM amitriptyline or with
877 10 µM ARC39 for 22 h (fresh inhibitor was applied after 18h) in infection medium. Then, cells were
878 washed thrice and lysed by addition of 100 µL per well ASM lysis buffer [250 mM NaOAc pH 5 (Roth,
879 Cat. No 6773.2), 0.1% Nonidet® P40 substitute (AppliChem. Cat. No. A1694,0250), 1.3 mM EDTA 1.3
880 mM (Roth, Cat. No. 8040.2), 1x protease inhibitor cocktail (Sigma Aldrich, 11873580001)] for 15
881 min/4°C. Cells were scraped from the substratum and protein concentration in the resulting lysates was
882 measured with a Pierce™ bicinchoninic acid (BCA) assay kit (Thermo Fisher, Cat. No. 23227). 1 µg of
883 protein was incubated with 100 µL ASM lysate assay buffer [200 mM NaOAc pH 5 (Roth, Cat. No
884 6773.2), 0.02 % Nonidet® P40 substitute (AppliChem. Cat. No. A1694,0250), 500 mM NaCl (VWR,
885 Cat. No. 27810.364)] containing 0.58 µM BODIPY-FL-C_{12}-Sphingomyelin (Thermo Fisher, Cat. No.
886 D7711) for 4h at 37°C and 300 rpm.
887 For measuring bacterial SMase/NSM activity in *S. aureus* cultures, an overnight culture of the indicated
888 strain was grown in BHI medium, centrifuged 14.000xg and the supernatant was sterile filtered with 0.2
889 µm filter. 100 µL of sterile supernatant was incubated with 100 µL NSM assay buffer [200 mM HEPES,
890 pH 7.0 (Roth, Cat. No. 6763.3), 200 mM $MgCl_2$ (Roth, Cat.No. 2189.2), 0.05% Nonidet P-40
891 (AppliChem. Cat. No. A1694,0250)] for 4h/37°C/300 rpm.
892 The reactions were stopped by the addition of 2:1 $CHCl_3$:MeOH (Roth, Cat. No. 3313.2 and Cat. No.
893 8388.6). Samples were vortexed, centrifuged at 13,000 x g for 3 min and 50-100 µL of the lower organic
894 phase were transferred to a fresh tube. Samples were completely evaporated using a SpeedVac 5301
895 concentrator (Eppendorf), resuspended in 10 µL 2:1 $CHCl_3$/MeOH and spotted in 2.5 µL aliquots on a
896 TLC plate (Alugram, Xtra Sil G/UV254, 0.2 mm/silica gel 60; VWR, Cat. No. 552-1006).
897 Plates were developed using 80:20 $CHCl_3$:MeOH and subsequently scanned with a Typhoon 9200
898 Scanner (Amersham). For quantification, intensities of the lower (SM) and the upper bands (Cer) were

899 measured in Fiji (109) and activity was determined based on the reaction time, protein amount and
900 SM/Cer ratios.
901 For the flow cytometry based read out, cells seeded in a density of $0.5x10^5$ cells per well in a 24 well
902 plate either one day (HeLa, EA.hy 926, 16HBE14o$^-$) or two days (HuLEC, HuVEC) prior to the
903 experiment. Cells were treated with ARC39 and amitriptyline as described above. Then, cells were
904 washed thrice with DPBS and incubated with 10 µM FRET probe (73) for 2h in presence of the
905 inhibitors. Subsequently, cells were washed thrice, detached with TrypLE^{TM} (Gibco^{TM}, Cat. No.
906 12604013) and resuspended with 2% (v/v) FBS in DPBS. Samples were analyzed for FITC (Ex. 488
907 nm/Em. band pass 530/30 nm) and BODIPY-TR (Ex.: 561nm/ Em. band pass 695/40nm) fluorescence
908 with Attune NxT flow cytometer (Thermo Fisher, Attune Cytometric Software v5.2.0). Cell populations
909 were analyzed for FITC and BODIPY-TR mean fluorescence in Flowing 2 (Turku Bioscience Center)
910 and FITC vs. BODIPY-TR ratios were calculated to determine arbitrary probe conversion.
911
912 **Determination of β-toxin activity on living cells**
913 HeLa cells were seeded in a 24 well plate with a density of $0.5x10^5$ cells per well. Cells were incubated
914 with 1 µM BODIPY-FL-C_{12}-SM for 24h. Then, samples were washed thrice with DPBS and treated
915 with 100 ng/ml β-toxin in infection medium or left untreated for 75 min. Subsequently, cells were
916 washed thrice with DPBS, lysed with 200 µL MeOH and detached with a cell scraper. 400 µL $CHCl_3$
917 and samples were centrifuged for 5 min/25.000xg to remove cell debris. 100 µL of the sample were
918 completely evaporated using a SpeedVac 5301 concentrator (Eppendorf), resuspended in 10 µL 2:1
919 $CHCl_3$/MeOH and spotted in 2.5 µL aliquots on a TLC plate (Alugram, Xtra Sil G/UV254, 0.2 mm/silica
920 gel 60; VWR, Cat. No. 552-1006). TLC was developed with 80:20 $CHCl_3$:MeOH and scanned with a
921 Typhoon RGB scanner (Amersham). Fluorescence intensities were evaluated in Fiji and ratios ceramide
922 vs. SM were calculated.
923
924 **Construction of HiBit-SP-LAMP1-p2A-eYFP.**
925 To visualize the transient surface exposure of lysosomal membranes on the plasma membrane of
926 epithelial cells we made use of a split NanoLuc luciferase. We inserted a region encoding the 11 amino
927 acid residues encompassing HiBiT peptide of the split NanoLuc (Promega) between the signal peptide
928 and the N-terminus of mature LAMP1.
929 For that purpose, we amplified a 144 bp fragment encoding the signal peptide of LAMP1 (SP_{LAMP1},
930 PmeInfus-SPLamp-fwd & LAMP1SP-HiBiT-r), the 1.2 kb coding region of mature LAMP1 (mLAMP1,
931 Inf-HiBiT-LAMP-f & LAMP1-as) and eYFP (cYFP-f & LV-Spe-rev) via PCR using the indicated
932 primer pairs respectively and using LAMP1-YFP containing plasmid as DNA template (41). A p2A
933 peptide encoding sequence was amplified with oligonucleotides Lamp1-p2a-f and p2a-eYFP-r using
934 pspCas9 (74) as a template. As vector we used the PmeI/SpeI-restricted pLVTHM (101).
935 The resulting DNA Fragments contained overlapping ends of at least 16 bp, which were assembled by
936 an InFusion enzyme mix (Takara Biotech) according to the manufacturer 's instructions. The resulting
937 plasmid was transformed into chemically competent *E. coli* DH5α and plated on LB agar containing
938 100 µg/ml ampicillin. Colonies were inoculated, and plasmid were prepared from the resulting overnight
939 cultures using the Qiagen Plasmid Mini kit. Sequences were determined using Sanger sequencing
940 (Microsynth) thereby establishing the correct assembly of the vector. Pseudotyped lentivirus particles
941 were generated in HEK293 cells and transduction of HeLa cells was conducted following a published
942 protocol (101).
943 eYFP production in transgenic cells here served as reporter for transfection of the cells and production
944 of the SP-HiBiT-LAMP1 proportion of the fusion protein. eYFP-positive cells were FACS-sorted for
945 medium eYFP expression levels and the resulting cell pool was named HeLa SP_{LAMP}1-HiBit-LAMP1-
946 p2A-EYFP.
947

948 **Determination of externalization of lysosomal membranes using split NanoLuc biolumin-escence.**
949 For measurement of LAMP1 externalization, $4x10^4$ per well of HeLa SP_{LAMP}1-HiBit-LAMP1-p2A-
950 EYFP, hereafter named HeLa HiBiT-LAMP1, were seeded in white flat-bottom 96 well plates (Nunc™
951 MicroWell™ 96 Wells, Nunclon Delta-treated, Cat. No. 136101) and grown overnight yielding $8x10^4$
952 cells at the next day. Bioluminescence was detected using the Promega Nano-Glo HiBiT Extracellular
953 Detection Kit (Promega # N2420).
954 For infection with *S. aureus*, bacteria from an overnight culture were diluted to an OD600 of
955 approximately 0.5 into 10 ml TSB and grown for 1 h. In case a preincubation with inhibitors was
956 required (e.g. as for vacuolin-1), cells were washed twice with DPBS, and inhibitors were added in
957 indicated concentrations in a final volume of 200 µl per well.
958 Extracellular detection reagent was prepared by mixing 4 ml extracellular buffer, 20 µl LgBit protein
959 and 40 µl bioluminescent substrate [Promega, Cat. No. N2420]. 100 µl extracellular detection reagent
960 was added per well and luminescence was measured five times in 2 min intervals on a TECAN Infinite
961 Pro 200 plate reader (37 °C, attenuation: OD1, integration time 250 ms). Then, inhibitors or bacteria
962 were added accordingly, and luminescence measurements were continued in 2 min intervals using the
963 settings above. The relative luminescence units (RLUs) determined in samples infected with *S. aureus*
964 were scaled to the untreated control (set to 0%) and cells treated with 1 µM ionomycin (set to 100 %).
965 The results describe the LAMP1 externalization as proportion of all lysosomes that can be released from
966 host cells by ionomycin treatment.
967
968 **Determination of cellular sphingolipid profiles via HPLC-MS/MS**
969 HeLa wildtype or ASM K.O. cells were seeded with a density of $3.5x10^6$ cells per well in a 6-well plate.
970 wildtype cells were treated as described in **Table 3** with 10 µM ARC39 or 20 µM amitriptyline. Then,
971 cells were washed thrice with DPBS, lysed with 250 µL cold MeOH and detached with a cell scraper
972 on ice. Wells were rinsed with an additional 250 µL MeOH to ensure entire sample collection.
973 Cell suspensions were then subjected to lipid extraction using 1 mL MeOH/$CHCl_3$ (2:1, v:v) as described
974 before (110). The extraction solvent contained C17 ceramide (C17 Cer) and d_{31}-C16 sphingomyelin
975 (d_{31}-C16 SM) (both Avanti Polar Lipids, Alabaster, USA) as internal standards. Chromatographic
976 separations were achieved on a 1290 Infinity II HPLC (Agilent Technologies, Waldbronn, Germany)
977 equipped with a Poroshell 120 EC-C8 column (3.0 × 150 mm, 2.7 µm; Agilent Technologies). MS/MS
978 analyses were carried out using a 6495C triple-quadrupole mass spectrometer (Agilent Technologies)
979 operating in the positive electrospray ionization mode (ESI+). Cer and SM were quantified by multiple
980 reaction monitoring (qualifier product ions in parentheses): $[M-H_2O+H]^+ \rightarrow m/z$ 264.3 (282.3) for all
981 Cer and $[M+H]^+ \rightarrow m/z$ 184.1 (86.1) for all SM subspecies (C16, C18, C20, C22, C24 and C24:1) (110).
982 Peak areas of Cer and SM subspecies, as determined with MassHunter Quantitative Analysis software
983 (version 10.1, Agilent Technologies), were normalized to those of the internal standards (C17 Cer or
984 d_{31}-C16 SM) followed by external calibration in the range of 1 fmol to 50 pmol on column.
985
986 **Cytotoxicity Assays**
987 For all cytotoxicity assays, HuLEC were seeded in 24 well plates with a density of $0.5x10^5$ cells per
988 well two days prior to the experiment. Then, cells were infected with *S. aureus* JE2 with the indicated
989 MOI as described in "*S. aureus* infection" and cytotoxicity was determined 21 h p.i. For cytotoxicity
990 measurements upon ionomycin treatment, cells were incubated with the indicated concentration of
991 ionomycin in infection medium for 75 min and then, cytotoxicity assays were conducted.
992 Lactate dehydrogenase (LDH) assay was performed with the Cytotoxicity Detection KitPLUS (LDH,
993 Sigma Aldrich, Cat. No. 4744934001) according to manufacturer's instructions.
994 For annexin V and 7-Aminoactinomycin D (7-AAD) assays, cells were washed thrice with DPBS,
995 detached with 250 µL per well trypsin and resuspended in 250 µL per well staining buffer [1.7% (v/v)
996 APC Annexin V (BD Pharmingen™, Cat. No. 550475), 1.7% (v/v) 7-AAD (BD Pharmingen™, Cat No.
997 559925), 2% (v/v) heat-inactivated (56°C/30 min) FBS (Sigma Aldrich, Cat. No. F7524), 4 mM $CaCl_2$

998 (Roth, Cat. No. 5239.1) in DPBS]. After incubation for 10 min/RT, cells were analyzed with an Attune
999 NxT flow cytometer for 7-AAD (Ex. 488 nm/Em. band pass 695/40 nm) and APC (Ex. 637 nm/Em.
1000 band pass 670/14 nm). Cell populations were analyzed with Flowing2 (Turku Biosciences Center) and
1001 gates were adjusted according to untreated control cells. To determine the proportion of cells that
1002 remained attached to the substratum during the infection, the number of cells was determined based on
1003 the number of detected single cells, flow rate and sample volume.
1004
1005 **Statistical analysis**
1006 Statistical analysis was performed in GraphPad prism (V10.1.2). One-sample t-test was used for analysis
1007 of normalized data sets. Otherwise, one- or two-way ANOVA, dependent on the number of variables,
1008 was used in combination with appropriate multiple comparisons testing. Details about sample size and
1009 corresponding statistical analysis can be found in respective figure legends. All data are shown as mean
1010 ± standard deviation.
1011
1012

References

1. Y. A. Hannun, L. M. Obeid, Sphingolipids and their metabolism in physiology and disease. *Nature Reviews Molecular Cell Biology* **19**, 175-191 (2018).
2. G. van Meer, D. R. Voelker, G. W. Feigenson, Membrane lipids: where they are and how they behave. *Nat Rev Mol Cell Biol* **9**, 112-124 (2008).
3. K. Segawa, J. Suzuki, S. Nagata, Flippases and scramblases in the plasma membrane. *Cell Cycle* **13**, 2990-2991 (2014).
4. R. O. Brady, J. N. Kanfer, M. B. Mock, D. S. Fredrickson, The metabolism of sphingomyelin. II. Evidence of an enzymatic deficiency in Niemann-Pick diseae. *Proc Natl Acad Sci U S A* **55**, 366-369 (1966).
5. B. Breiden, K. Sandhoff, Acid Sphingomyelinase, a Lysosomal and Secretory Phospholipase C, Is Key for Cellular Phospholipid Catabolism. *Int J Mol Sci* **22** (2021).
6. C. Tam *et al.*, Exocytosis of acid sphingomyelinase by wounded cells promotes endocytosis and plasma membrane repair. *J Cell Biol* **189**, 1027-1038 (2010).
7. M. C. Fernandes *et al.*, Trypanosoma cruzi subverts the sphingomyelinase-mediated plasma membrane repair pathway for cell invasion. *J Exp Med* **208**, 909-921 (2011).
8. S. Peters *et al.*, Neisseria meningitidis Type IV Pili Trigger Ca(2+)-Dependent Lysosomal Trafficking of the Acid Sphingomyelinase To Enhance Surface Ceramide Levels. *Infect Immun* **87** (2019).
9. R. W. Jenkins *et al.*, Regulated Secretion of Acid Sphingomyelinase: IMPLICATIONS FOR SELECTIVITY OF CERAMIDE FORMATION*. *Journal of Biological Chemistry* **285**, 35706-35718 (2010).
10. J. Kornhuber, C. Rhein, C. P. Muller, C. Muhle, Secretory sphingomyelinase in health and disease. *Biol Chem* **396**, 707-736 (2015).
11. Krones & Rühling *et al.*, Staphylococcus aureus alpha-Toxin Induces Acid Sphingomyelinase Release From a Human Endothelial Cell Line. *Front Microbiol* **12**, 694489 (2021).
12. S. L. Schissel *et al.*, Secretory sphingomyelinase, a product of the acid sphingomyelinase gene, can hydrolyze atherogenic lipoproteins at neutral pH. Implications for atherosclerotic lesion development. *J Biol Chem* **273**, 2738-2746 (1998).
13. C. Li *et al.*, Regulation of Staphylococcus aureus Infection of Macrophages by CD44, Reactive Oxygen Species, and Acid Sphingomyelinase. *Antioxid Redox Signal* **28**, 916-934 (2018).
14. H. Grassme *et al.*, Acidic sphingomyelinase mediates entry of N. gonorrhoeae into nonphagocytic cells. *Cell* **91**, 605-615 (1997).
15. A. Carpinteiro *et al.*, Pharmacological Inhibition of Acid Sphingomyelinase Prevents Uptake of SARS-CoV-2 by Epithelial Cells. *Cell Rep Med* **1**, 100142 (2020).
16. S. Luisoni *et al.*, Co-option of Membrane Wounding Enables Virus Penetration into Cells. *Cell Host & Microbe* **18**, 75-85 (2015).
17. E. Avota, E. Gulbins, S. Schneider-Schaulies, DC-SIGN mediated sphingomyelinase-activation and ceramide generation is essential for enhancement of viral uptake in dendritic cells. *PLoS Pathog* **7**, e1001290 (2011).
18. A. Sakr, F. Brégeon, J. L. Mège, J. M. Rolain, O. Blin, Staphylococcus aureus Nasal Colonization: An Update on Mechanisms, Epidemiology, Risk Factors, and Subsequent Infections. *Front Microbiol* **9**, 2419 (2018).
19. L. F. McCaig, L. C. McDonald, S. Mandal, D. B. Jernigan, Staphylococcus aureus-associated skin and soft tissue infections in ambulatory care. *Emerg Infect Dis* **12**, 1715-1723 (2006).
20. L. Liesenborghs *et al.*, Staphylococcus aureus endocarditis: distinct mechanisms of bacterial adhesion to damaged and inflamed heart valves. *Eur Heart J* **40**, 3248-3259 (2019).
21. J. A. Silversides, E. Lappin, A. J. Ferguson, Staphylococcal toxic shock syndrome: mechanisms and management. *Curr Infect Dis Rep* **12**, 392-400 (2010).
22. C. Antimicrobial Resistance, Global burden of bacterial antimicrobial resistance in 2019: a systematic analysis. *Lancet* **399**, 629-655 (2022).
23. M. Fraunholz, B. Sinha, Intracellular Staphylococcus aureus: live-in and let die. *Front Cell Infect Microbiol* **2**, 43 (2012).

24. I. Rodrigues Lopes *et al.*, Microscopy-based phenotypic profiling of infection by Staphylococcus aureus clinical isolates reveals intracellular lifestyle as a prevalent feature. *Nature Communications* **13**, 7174 (2022).
25. J. W. Hommes, B. G. J. Surewaard, Intracellular Habitation of Staphylococcus aureus: Molecular Mechanisms and Prospects for Antimicrobial Therapy. *Biomedicines* **10**, 1804 (2022).
26. S. N. Qazi, S. E. Harrison, T. Self, P. Williams, P. J. Hill, Real-time monitoring of intracellular Staphylococcus aureus replication. *J Bacteriol* **186**, 1065-1077 (2004).
27. J. Abel *et al.*, Staphylococcus aureus evades the extracellular antimicrobial activity of mast cells by promoting its own uptake. *J Innate Immun* **3**, 495-507 (2011).
28. B. Sinha *et al.*, Fibronectin-binding protein acts as Staphylococcus aureus invasin via fibronectin bridging to integrin alpha5beta1. *Cell Microbiol* **1**, 101-117 (1999).
29. F. Agerer *et al.*, Cellular invasion by Staphylococcus aureus reveals a functional link between focal adhesion kinase and cortactin in integrin-mediated internalisation. *J Cell Sci* **118**, 2189-2200 (2005).
30. F. Agerer, A. Michel, K. Ohlsen, C. R. Hauck, Integrin-mediated invasion of Staphylococcus aureus into human cells requires Src family protein-tyrosine kinases. *J Biol Chem* **278**, 42524-42531 (2003).
31. Y. T. Ying *et al.*, Annexin A2-Mediated Internalization of Staphylococcus aureus into Bovine Mammary Epithelial Cells Requires Its Interaction with Clumping Factor B. *Microorganisms* **9** (2021).
32. S. L. Stroschein-Stevenson, E. Foley, P. H. O'Farrell, A. D. Johnson, Identification of Drosophila gene products required for phagocytosis of Candida albicans. *PLoS Biol* **4**, e4 (2006).
33. A. M. Towell *et al.*, Staphylococcus aureus binds to the N-terminal region of corneodesmosin to adhere to the stratum corneum in atopic dermatitis. *Proceedings of the National Academy of Sciences* **118**, e2014444118 (2021).
34. F. Askarian *et al.*, The interaction between Staphylococcus aureus SdrD and desmoglein 1 is important for adhesion to host cells. *Scientific Reports* **6**, 22134 (2016).
35. N. Bravo-Santano *et al.*, Host-directed kinase inhibitors act as novel therapies against intracellular Staphylococcus aureus. *Scientific Reports* **9**, 4876 (2019).
36. P. M. Tribelli *et al.*, Staphylococcus aureus Lpl protein triggers human host cell invasion via activation of Hsp90 receptor. *Cell Microbiol* **22**, e13111 (2020).
37. N. Hirschhausen *et al.*, A novel staphylococcal internalization mechanism involves the major autolysin Atl and heat shock cognate protein Hsc70 as host cell receptor. *Cell Microbiol* **12**, 1746-1764 (2010).
38. K. Dziewanowska *et al.*, Staphylococcal fibronectin binding protein interacts with heat shock protein 60 and integrins: role in internalization by epithelial cells. *Infect Immun* **68**, 6321-6328 (2000).
39. A. Moldovan, M. J. Fraunholz, In or out: Phagosomal escape of Staphylococcus aureus. *Cell Microbiol* **21**, e12997 (2019).
40. C. E. Jauregui, J. P. Mansell, M. A. Jepson, H. F. Jenkinson, Differential interactions of Streptococcus gordonii and Staphylococcus aureus with cultured osteoblasts. *Mol Oral Microbiol* **28**, 250-266 (2013).
41. B. Giese *et al.*, Staphylococcal alpha-toxin is not sufficient to mediate escape from phagolysosomes in upper-airway epithelial cells. *Infect Immun* **77**, 3611-3625 (2009).
42. M. Grosz *et al.*, Cytoplasmic replication of Staphylococcus aureus upon phagosomal escape triggered by phenol-soluble modulin alpha. *Cell Microbiol* **16**, 451-465 (2014).
43. J. Horn, K. Stelzner, T. Rudel, M. Fraunholz, Inside job: Staphylococcus aureus host-pathogen interactions. *Int J Med Microbiol* **308**, 607-624 (2018).
44. R. Wang *et al.*, Identification of novel cytolytic peptides as key virulence determinants for community-associated MRSA. *Nat Med* **13**, 1510-1514 (2007).
45. K. Stelzner *et al.*, Intracellular Staphylococcus aureus employs the cysteine protease staphopain A to induce host cell death in epithelial cells. *PLoS Pathog* **17**, e1009874 (2021).

46. J. Gatfield, J. Pieters, Essential role for cholesterol in entry of mycobacteria into macrophages. *Science* **288**, 1647-1650 (2000).
47. R. Zidovetzki, I. Levitan, Use of cyclodextrins to manipulate plasma membrane cholesterol content: evidence, misconceptions and control strategies. *Biochim Biophys Acta* **1768**, 1311-1324 (2007).
48. K. A. Joiner, S. A. Fuhrman, H. M. Miettinen, L. H. Kasper, I. Mellman, Toxoplasma gondii: Fusion Competence of Parasitophorous Vacuoles in Fc Receptor-Transfected Fibroblasts. *Science* **249**, 641-646 (1990).
49. S. Kim, M. Watarai, S.-i. Makino, T. Shirahata, Membrane sorting during swimming internalization of Brucella is required for phagosome trafficking decisions. *Microbial Pathogenesis* **33**, 225-237 (2002).
50. K. Stelzner *et al.*, Intracellular Staphylococcus aureus Perturbs the Host Cell Ca(2+) Homeostasis To Promote Cell Death. *mBio* **11** (2020).
51. R. Y. Tsien, A non-disruptive technique for loading calcium buffers and indicators into cells. *Nature* **290**, 527-528 (1981).
52. M. D. Bootman, G. Bultynck, Fundamentals of Cellular Calcium Signaling: A Primer. *Cold Spring Harb Perspect Biol* **12** (2020).
53. T. Maruyama, T. Kanaji, S. Nakade, T. Kanno, K. Mikoshiba, 2APB, 2-aminoethoxydiphenyl borate, a membrane-penetrable modulator of Ins(1,4,5)P3-induced Ca2+ release. *J Biochem* **122**, 498-505 (1997).
54. T. F. Walseth, H. C. Lee, Synthesis and characterization of antagonists of cyclic-ADP-ribose-induced Ca2+ release. *Biochim Biophys Acta* **1178**, 235-242 (1993).
55. E. Naylor *et al.*, Identification of a chemical probe for NAADP by virtual screening. *Nature Chemical Biology* **5**, 220-226 (2009).
56. S. Y. Kim, B. H. Cho, U. H. Kim, CD38-mediated Ca2+ signaling contributes to angiotensin II-induced activation of hepatic stellate cells: attenuation of hepatic fibrosis by CD38 ablation. *J Biol Chem* **285**, 576-582 (2010).
57. S. Y. Rah, M. Mushtaq, T. S. Nam, S. H. Kim, U. H. Kim, Generation of cyclic ADP-ribose and nicotinic acid adenine dinucleotide phosphate by CD38 for Ca2+ signaling in interleukin-8-treated lymphokine-activated killer cells. *J Biol Chem* **285**, 21877-21887 (2010).
58. Z. L. Piedra-Quintero, Z. Wilson, P. Nava, M. Guerau-de-Arellano, CD38: An Immunomodulatory Molecule in Inflammation and Autoimmunity. *Front Immunol* **11**, 597959 (2020).
59. C. Angeletti *et al.*, SARM1 is a multi-functional NAD(P)ase with prominent base exchange activity, all regulated bymultiple physiologically relevant NAD metabolites. *iScience* **25**, 103812 (2022).
60. F. Gu *et al.*, Dual NADPH oxidases DUOX1 and DUOX2 synthesize NAADP and are necessary for Ca(2+) signaling during T cell activation. *Sci Signal* **14**, eabe3800 (2021).
61. E. V. Caler, S. Chakrabarti, K. T. Fowler, S. Rao, N. W. Andrews, The Exocytosis-regulatory protein synaptotagmin VII mediates cell invasion by Trypanosoma cruzi. *J Exp Med* **193**, 1097-1104 (2001).
62. H. Grassmé, A. Riehle, B. Wilker, E. Gulbins, Rhinoviruses infect human epithelial cells via ceramide-enriched membrane platforms. *J Biol Chem* **280**, 26256-26262 (2005).
63. M. E. Miller, S. Adhikary, A. A. Kolokoltsov, R. A. Davey, Ebolavirus Requires Acid Sphingomyelinase Activity and Plasma Membrane Sphingomyelin for Infection. *Journal of Virology* **86**, 7473-7483 (2012).
64. M. P. Hall *et al.*, Engineered Luciferase Reporter from a Deep Sea Shrimp Utilizing a Novel Imidazopyrazinone Substrate. *ACS Chemical Biology* **7**, 1848-1857 (2012).
65. A. S. Dixon *et al.*, NanoLuc Complementation Reporter Optimized for Accurate Measurement of Protein Interactions in Cells. *ACS Chemical Biology* **11**, 400-408 (2016).
66. N. W. Andrews, "Detection of Lysosomal Exocytosis by Surface Exposure of Lamp1 Luminal Epitopes" in Lysosomes: Methods and Protocols, K. Öllinger, H. Appelqvist, Eds. (Springer New York, New York, NY, 2017), 10.1007/978-1-4939-6934-0_13, pp. 205-211.

67. A. Rodriguez, P. Webster, J. Ortego, N. W. Andrews, Lysosomes behave as Ca2+-regulated exocytic vesicles in fibroblasts and epithelial cells. *J Cell Biol* **137**, 93-104 (1997).
68. J. Cerny *et al.*, The small chemical vacuolin-1 inhibits Ca(2+)-dependent lysosomal exocytosis but not cell resealing. *EMBO Rep* **5**, 883-888 (2004).
69. A. Reddy, E. V. Caler, N. W. Andrews, Plasma membrane repair is mediated by Ca(2+)-regulated exocytosis of lysosomes. *Cell* **106**, 157-169 (2001).
70. H. Grassmé *et al.*, Acidic sphingomyelinase mediates entry of N. gonorrhoeae into nonphagocytic cells. *Cell* **91**, 605-615 (1997).
71. A. G. Roth *et al.*, Potent and selective inhibition of acid sphingomyelinase by bisphosphonates. *Angew Chem Int Ed Engl* **48**, 7560-7563 (2009).
72. C. Muhle, J. Kornhuber, Assay to measure sphingomyelinase and ceramidase activities efficiently and safely. *J Chromatogr A* **1481**, 137-144 (2017).
73. C. Kappe, Z. H. Mohamed, E. Naser, A. Carpinteiro, C. Arenz, A Novel Visible Range FRET Probe for Monitoring Acid Sphingomyelinase Activity in Living Cells. *Chemistry* **26**, 5780-5783 (2020).
74. F. A. Ran *et al.*, Genome engineering using the CRISPR-Cas9 system. *Nature Protocols* **8**, 2281-2308 (2013).
75. E. H. Schuchman, R. J. Desnick, Types A and B Niemann-Pick disease. *Mol Genet Metab* **120**, 27-33 (2017).
76. C. Hoffmann *et al.*, Caveolin limits membrane microdomain mobility and integrin-mediated uptake of fibronectin-binding pathogens. *J Cell Sci* **123**, 4280-4291 (2010).
77. L.-P. Tricou *et al.*, Staphylococcus aureus can use an alternative pathway to be internalized by osteoblasts in absence of β1 integrins. *Scientific Reports* **14**, 28643 (2024).
78. J. Rappaport, C. Garnacho, S. Muro, Clathrin-mediated endocytosis is impaired in type A-B Niemann-Pick disease model cells and can be restored by ICAM-1-mediated enzyme replacement. *Mol Pharm* **11**, 2887-2895 (2014).
79. J. Rappaport, R. L. Manthe, C. Garnacho, S. Muro, Altered Clathrin-Independent Endocytosis in Type A Niemann-Pick Disease Cells and Rescue by ICAM-1-Targeted Enzyme Delivery. *Mol Pharm* **12**, 1366-1376 (2015).
80. R. Pantůcek *et al.*, Identification of bacteriophage types and their carriage in Staphylococcus aureus. *Arch Virol* **149**, 1689-1703 (2004).
81. M. Rühling *et al.*, Trifunctional sphingomyelin derivatives enable nanoscale resolution of sphingomyelin turnover in physiological and infection processes via expansion microscopy. *Nature Communications* **15**, 7456 (2024).
82. C. J. Ellison, W. Kukulski, K. B. Boyle, S. Munro, F. Randow, Transbilayer Movement of Sphingomyelin Precedes Catastrophic Breakage of Enterobacteria-Containing Vacuoles. *Curr Biol* **30**, 2974-2983 e2976 (2020).
83. M. Rühling, F. Schmelz, A. Kempf, K. Paprotka, J. Fraunholz Martin, Identification of the Staphylococcus aureus endothelial cell surface interactome by proximity labeling. *mBio* **0**, e03654-03624 (2025).
84. F. Falugi, H. K. Kim, D. M. Missiakas, O. Schneewind, Role of protein A in the evasion of host adaptive immune responses by Staphylococcus aureus. *mBio* **4**, e00575-00513 (2013).
85. A. J. Morgan, R. Jacob, Ionomycin enhances Ca2+ influx by stimulating store-regulated cation entry and not by a direct action at the plasma membrane. *Biochem J* **300 (Pt 3)**, 665-672 (1994).
86. O. Sano *et al.*, Vacuolin-1 inhibits autophagy by impairing lysosomal maturation via PIKfyve inhibition. *FEBS Letters* **590**, 1576-1585 (2016).
87. J.-S. Schonn, A. Maximov, Y. Lao, T. C. Südhof, J. B. Sørensen, Synaptotagmin-1 and -7 are functionally overlapping Ca²⁺ sensors for exocytosis in adrenal chromaffin cells. *Proceedings of the National Academy of Sciences* **105**, 3998-4003 (2008).
88. A. J. Morgan, F. M. Platt, E. Lloyd-Evans, A. Galione, Molecular mechanisms of endolysosomal Ca2+ signalling in health and disease. *Biochemical Journal* **439**, 349-378 (2011).

1221 89. L. C. Davis, A. J. Morgan, A. Galione, NAADP-regulated two-pore channels drive phagocytosis
1222 through endo-lysosomal Ca(2+) nanodomains, calcineurin and dynamin. *EMBO J* **39**, e104058
1223 (2020).
1224 90. Y. Sakurai *et al.*, Ebola virus. Two-pore channels control Ebola virus host cell entry and are drug
1225 targets for disease treatment. *Science* **347**, 995-998 (2015).
1226 91. G. S. Gunaratne, Y. Yang, F. Li, T. F. Walseth, J. S. Marchant, NAADP-dependent Ca(2+) signaling
1227 regulates Middle East respiratory syndrome-coronavirus pseudovirus translocation through
1228 the endolysosomal system. *Cell Calcium* **75**, 30-41 (2018).
1229 92. X. Ou *et al.*, Characterization of spike glycoprotein of SARS-CoV-2 on virus entry and its immune
1230 cross-reactivity with SARS-CoV. *Nature Communications* **11**, 1620 (2020).
1231 93. L. C. Davis *et al.*, NAADP activates two-pore channels on T cell cytolytic granules to stimulate
1232 exocytosis and killing. *Curr Biol* **22**, 2331-2337 (2012).
1233 94. A. Arredouani *et al.*, Nicotinic Acid Adenine Dinucleotide Phosphate (NAADP) and
1234 Endolysosomal Two-pore Channels Modulate Membrane Excitability and Stimulus-Secretion
1235 Coupling in Mouse Pancreatic β Cells. *J Biol Chem* **290**, 21376-21392 (2015).
1236 95. C. R. Bollinger, V. Teichgräber, E. Gulbins, Ceramide-enriched membrane domains. *Biochimica*
1237 *et Biophysica Acta (BBA) - Molecular Cell Research* **1746**, 284-294 (2005).
1238 96. Y. Zhang, X. Li, K. A. Becker, E. Gulbins, Ceramide-enriched membrane domains—Structure and
1239 function. *Biochimica et Biophysica Acta (BBA) - Biomembranes* **1788**, 178-183 (2009).
1240 97. R. S. Flannagan, R. C. Kuiack, M. J. McGavin, D. E. Heinrichs, Staphylococcus aureus Uses the
1241 GraXRS Regulatory System To Sense and Adapt to the Acidified Phagolysosome in
1242 Macrophages. *mBio* **9** (2018).
1243 98. H. Peng *et al.*, Acid sphingomyelinase inhibition protects mice from lung edema and lethal
1244 Staphylococcus aureus sepsis. *J Mol Med (Berl)* **93**, 675-689 (2015).
1245 99. J. Kornhuber *et al.*, Functional Inhibitors of Acid Sphingomyelinase (FIASMAs): a novel
1246 pharmacological group of drugs with broad clinical applications. *Cell Physiol Biochem* **26**, 9-20
1247 (2010).
1248 100. S. Kimura, T. Noda, T. Yoshimori, Dissection of the autophagosome maturation process by a
1249 novel reporter protein, tandem fluorescent-tagged LC3. *Autophagy* **3**, 452-460 (2007).
1250 101. M. Wiznerowicz, D. Trono, Conditional suppression of cellular genes: lentivirus vector-
1251 mediated drug-inducible RNA interference. *J Virol* **77**, 8957-8961 (2003).
1252 102. V. Hung *et al.*, Proteomic mapping of cytosol-facing outer mitochondrial and ER membranes in
1253 living human cells by proximity biotinylation. *eLife* **6**, e24463 (2017).
1254 103. C. J. Edgell, C. C. McDonald, J. B. Graham, Permanent cell line expressing human factor VIII-
1255 related antigen established by hybridization. *Proceedings of the National Academy of Sciences*
1256 **80**, 3734-3737 (1983).
1257 104. S. Blättner *et al.*, Staphylococcus aureus Exploits a Non-ribosomal Cyclic Dipeptide to Modulate
1258 Survival within Epithelial Cells and Phagocytes. *PLOS Pathogens* **12**, e1005857 (2016).
1259 105. J. M. Vann, R. A. Proctor, Ingestion of Staphylococcus aureus by bovine endothelial cells results
1260 in time- and inoculum-dependent damage to endothelial cell monolayers. *Infect Immun* **55**,
1261 2155-2163 (1987).
1262 106. P. D. Fey *et al.*, A genetic resource for rapid and comprehensive phenotype screening of
1263 nonessential *Staphylococcus aureus* genes. *MBio* **4**, e00537-00512 (2013).
1264 107. K. A. Becker *et al.*, Staphylococcus aureus Alpha-Toxin Disrupts Endothelial-Cell Tight Junctions
1265 via Acid Sphingomyelinase and Ceramide. *Infect Immun* **86** (2018).
1266 108. B. Giese *et al.*, Expression of δ-toxin by Staphylococcus aureus mediates escape from phago-
1267 endosomes of human epithelial and endothelial cells in the presence of β-toxin. *Cell Microbiol*
1268 **13**, 316-329 (2011).
1269 109. J. Schindelin *et al.*, Fiji: an open-source platform for biological-image analysis. *Nat Methods* **9**,
1270 676-682 (2012).
1271 110. A. Prell, D. Wigger, A. Huwiler, F. Schumacher, B. Kleuser, The sphingosine kinase 2 inhibitors
1272 ABC294640 and K145 elevate (dihydro)sphingosine 1-phosphate levels in various cells. *J Lipid*
1273 *Res* **65**, 100631 (2024).

Supplementary Figures

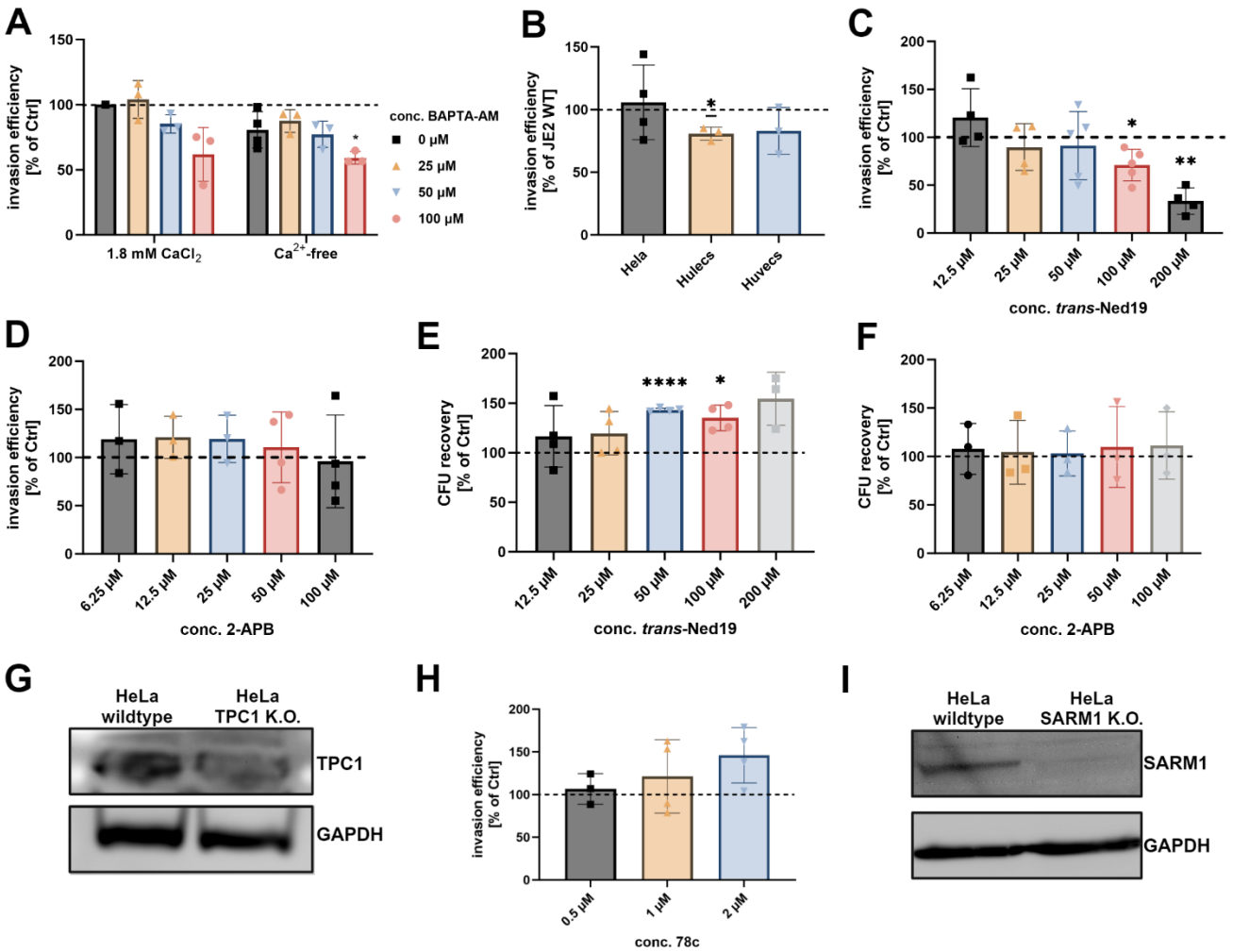

Supp. Figure 1 Supporting information for Ca^{2+}-dependent internalization of *S. aureus*.
. (**A**) **Chelation of intracellular but not presence of extracellular Ca^{2+} affects *S. aureus* internalization by HeLa cells.** HeLa cells were preloaded with varying concentrations of the cell-permeable Ca^{2+} chelator BAPTA-AM and then infected with *S. aureus* JE2 in presence (+1.8 mM $CaCl_2$) or absence (Ca^{2+}-free) of Ca^{2+} in the cell culture medium. Invasion efficiency was determined by CFU plating. (**B**) **α-toxin plays only a subordinate role during *S. aureus* uptake by host cells.** HeLa, HuLEC or HuVEC were infected with *S. aureus* JE2 wildtype or a strain deficient in α-toxin production (Δ*hla*). Invasion efficiency was determined by CFU plating. The number of intracellular bacteria was normalized to samples infected with the wildtype. (**C, D**) ***trans*-Ned19 but not 2-APB affects invasion of *S. aureus* JE2 in HeLa.** HeLa cells were pre-treated with *trans*-Ned19 (**C**) or 2-APB (**D**). 2-APB was removed from the cells shortly before infection to avoid direct contact of inhibitor and bacteria (due to a bactericidal effect of 2-APB; data not shown). Then, cells were infected with *S. aureus* JE2 and invasion efficiency was determined. (**E, F**) ***trans*-Ned19 and 2-APB have no effect on *S. aureus* JE2 in our infection protocol.** HeLa cells were pre-treated with or 2-APB (**E**) or *trans*-Ned19 (**F**). 2-APB was removed from the cells shortly before infection. Then, cells were infected with *S. aureus* JE2 and, after 30 min, total bacteria (extra- and intracellular) were recovered by CFU plating. (**G**) **Reduction of TPC1 expression in a Cas9-treated cell pool (HeLa TPC1 K.O.).** TPC1 as well as GAPDH (loading control) was detected in lysates of wildtype and TPC1 K.O. cells via Western blot. (**H**) **CD38 is not involved in *S. aureus* internalization.** HeLa cells were pretreated with the CD38 inhibitor 78c and invasion efficiency of *S. aureus* JE2 was determined. (**I**) **Reduction of SARM1 expression in a Cas9-treated cell pool (HeLa SARM1 K.O.).** TPC1 as well as GAPDH (loading control) was detected in lysates of wildtype and SARM1 K.O. cells via Western blot. Statistics: one sample t-test, Bars represent mean +/- SD. *$p \leq 0.05$, **$p \leq 0.01$, ***$p \leq 0.001$, ****$p \leq 0.0001$.

1300

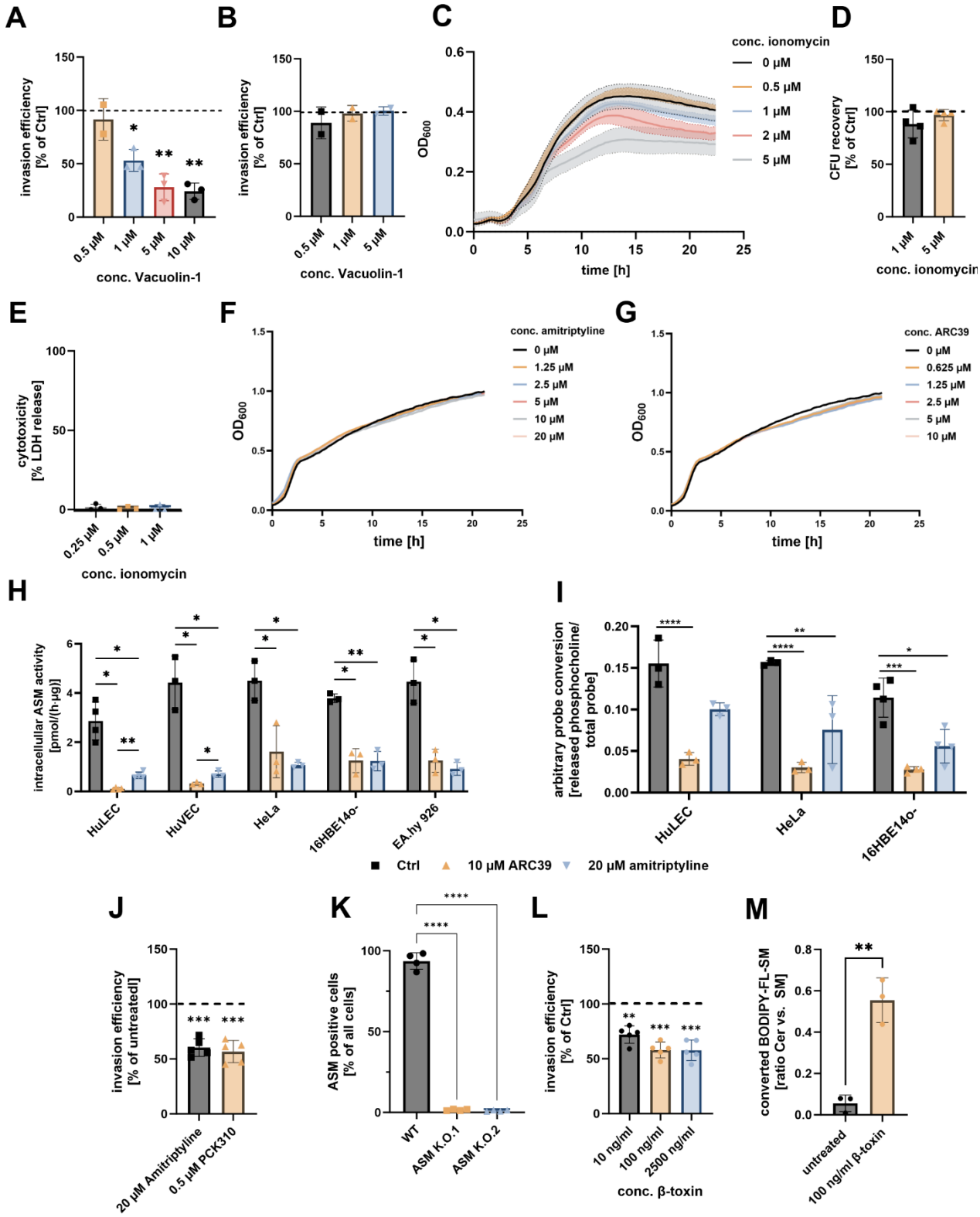

Supp. Figure 2 Supporting information for the involvement of lysosomal exocytosis and ASM in *S. aureus* invasion

(A) High ionomycin concentrations interfere with growth of *S. aureus* JE2. *S. aureus* JE2 was grown in in presence of varying concentrations of ionomycin. Growth (OD_{600}) was determined in a microplate reader. **(B) Ionomycin does not affect survival of *S. aureus* JE2 during infection of host cells.** HeLa cells were pretreated with varying concentrations of ionomycin and subsequently, infected with *S. aureus* JE2. After 30 min, cells were lysed and surviving extra- and intracellular bacteria were recovered by CFU count. **(C) Ionomycin does not affect host cell survival.** HeLa cells were treated with the indicated concentrations of ionomycin, and cytotoxicity was determined by measuring in lactate dehydrogenase (LDH) release. **(D)**

Blocking lysosomal exocytosis by Vacuolin-1 reduces *S. aureus* invasion in HeLa. HeLa cells were treated with increasing concentrations of the lysosomal exocytosis inhibitor Vacuolin-1. The invasion efficiency of *S. aureus* JE2 was determined 30 min p.i. **(E) Vacuolin-1 has no bactericidal effect.** HeLa cells were treated with Vacuolin-1 and infected with *S. aureus* JE2. After 30 min, total bacteria (extra- and intracellular) were recovered by CFU plating and normalized to untreated controls. **(F, G) The ASM inhibitors amitriptyline and ARC39 have no effect on growth of *S. aureus*.** *S. aureus* JE2 was grown in presence of varying concentrations of amitriptyline (**F**) or ARC39 (**G**) in BHI medium and growth was determined by measuring OD_{600} in a microplate reader. **(H, I) ASM activity and ASM inhibition by ARC39 and amitriptyline are similar among human cell lines.** Several cell lines were treated with amitriptyline or ARC39 and ASM activity within cell lysates was assessed by either thin layer chromatography-based ASM activity assays, detecting the conversion of BODIPY-C12-SM (**H**), or by a flow cytometry-based ASM activity assay and conversion of visible-range FRET probe (**I**). **(J) Microscopy-based measurement of invasion efficiency in amitriptyline- and PCK310-treated Hela cells.** Hela cells were treated with 20 µM amitriptyline (75 min) or 0.5 µM PCK310 (4h) and infected with *S. aureus* JE2 expressing Cerulean. Number of intracellular bacteria per host cell was determined by CLSM. n=5. **(K) Validation of ASM K.O. cell pools.** ASM activity in HeLa wildytpe or ASM K.O.s was determined with the visible-range FRET probe and flow cytometry. The proportion of ASM-positive cells in the cell population was determined. n=4. **(L) Removal of SM from the plasma membrane by β-toxin affects *S. aureus* host cell entry in HeLa.** HeLa cells were pretreated with the indicated concentrations of β-toxin and subsequently the invasion efficiency of *S. aureus* JE2 was determined. **(M) Treatment of HeLa with the bacterial SMases β-toxin results in generation of ceramide.** HeLa cells were preloaded with 1 µM BODIPY-FL-C_{12}-SM and treated with β-toxin for 75 min. Quantities of ceramide and SM were determined by TLC and ratio of ceramide vs. SM were calculated. Statistics: one sample t-test (D, J, L), mixed-effects model (REML) and Tukey`s multiple comparison (H, I), one-way ANOVA and Dunnett`s multiple comparison (K), unpaired Student´s t-test (M). Bars represent mean +/- SD. *$p \leq 0.05$, **$p \leq 0.01$, ***$p \leq 0.001$, ****$p \leq 0.0001$.

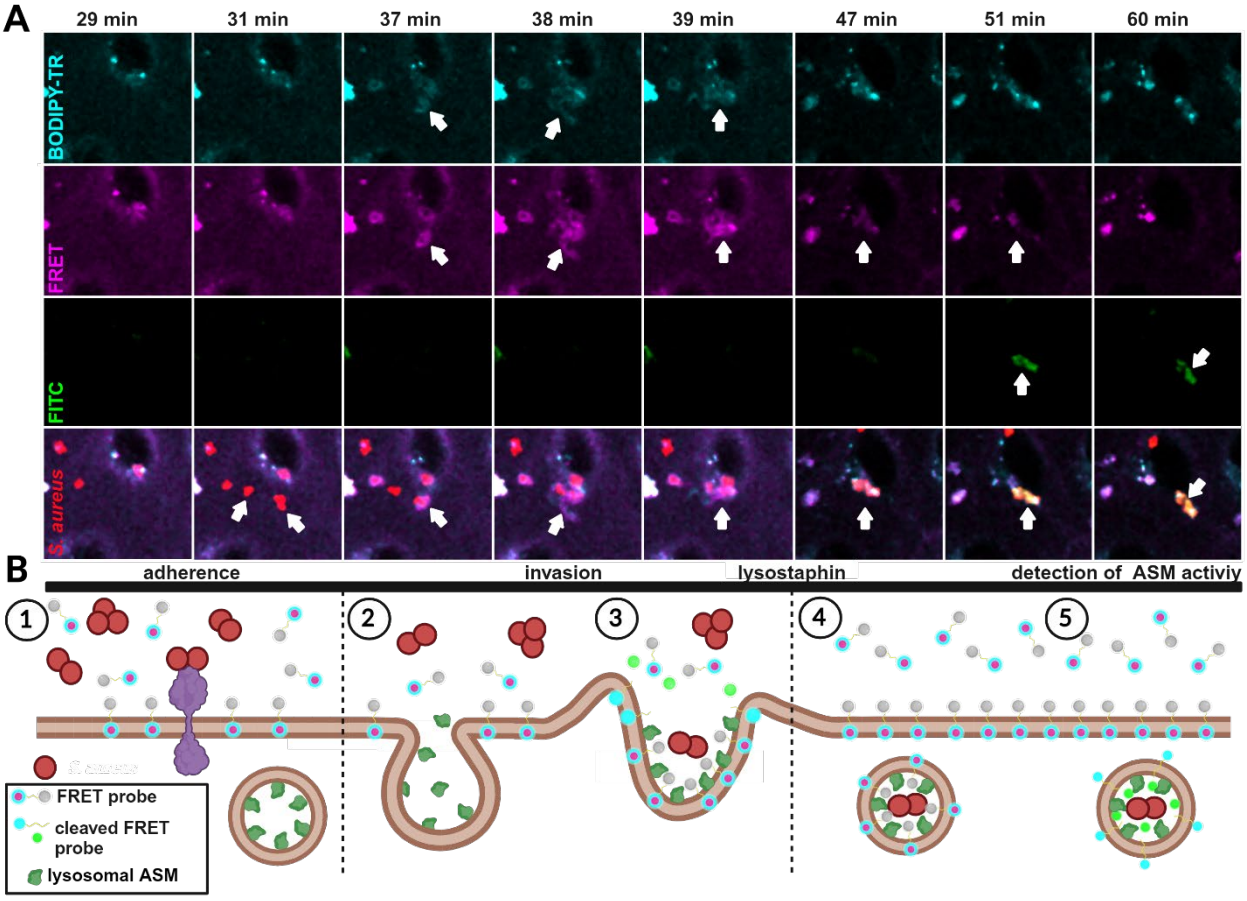

Supp. Figure 3 *S. aureus* associates with a visible-range SM probe during host cell invasion.
(A) Live cell imaging of *S. aureus* infection reveals association of the bacteria with a SM analog during cell entry. HuLEC were treated with 10 µM of a visible range FRET probe in presence of 1% FBS. Then, cells were infected with *S. aureus* JE2 in presence of the probe and infection was monitored by live cell confocal imaging. After 40 min, lysostaphin was added to remove extracellular bacteria. The BODIPY-TR signal demonstrates the localization of the probe, the FRET signal indicates an intact, non-metabolized probe, whereas FITC fluorescence indicates probe cleavage by ASM. Bacteria of interest (white arrows) adhere to host cell between 29 and 31 min p.i. **(B) Hypothetical model of *S. aureus* invasion.** (1). The interaction of bacteria with the host cell surface triggers lysosomal exocytosis, release of ASM (2) and the uptake of the bacteria (cmp. to A: at 37-39 min p.i.) by ASM-dependent membrane remodeling (3). ASM is co-internalized together with bacteria (4) and subsequently, cleaves the probe within the *S. aureus*-containing phagosome (5) (cmp: to A: increasing FITC signal starting at 47 min p.i.).

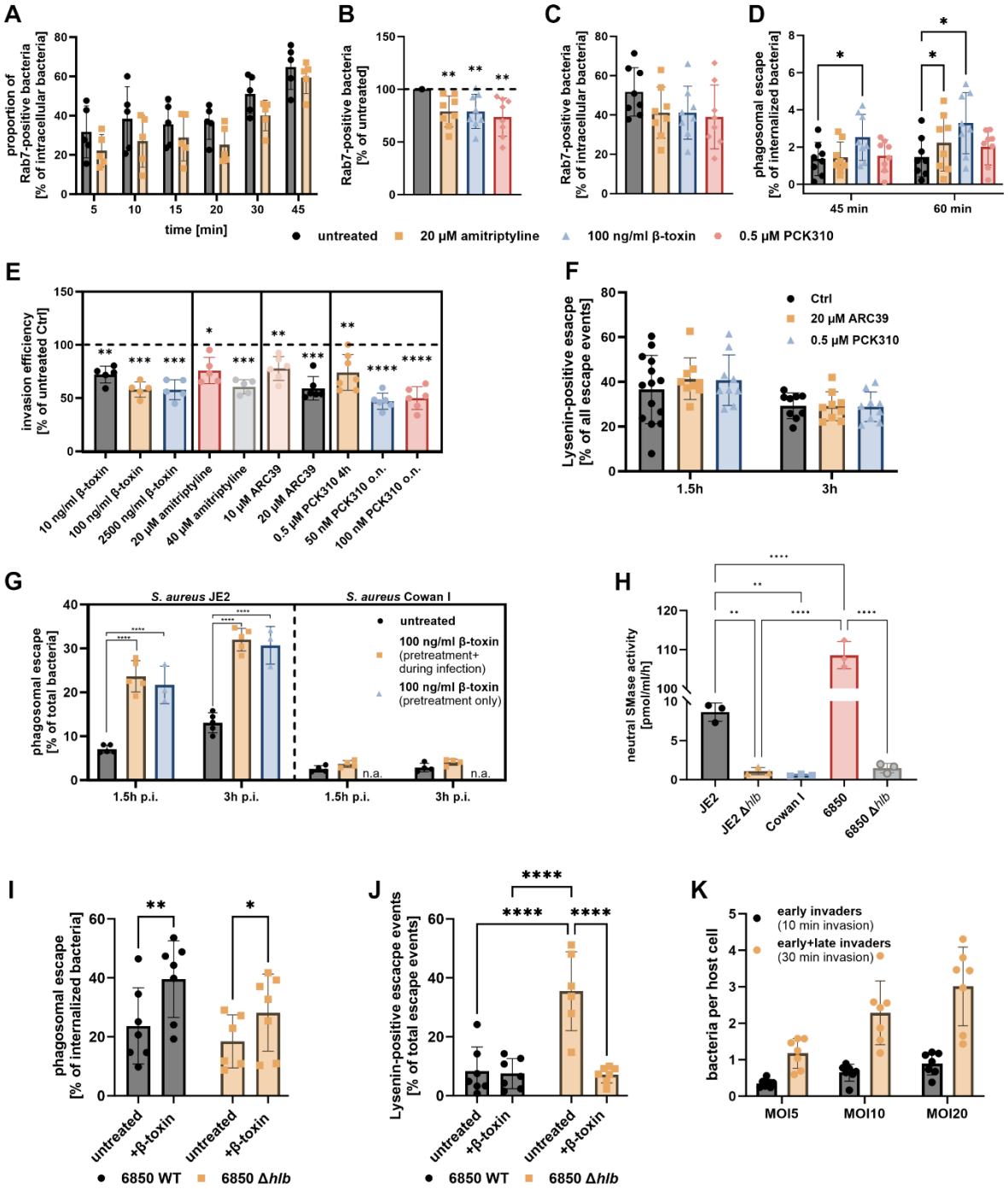

Supp. Figure 4 Supporting information for phagosomal maturation and phagosomal escape measurements.

(A) amitriptyline treatment reduces the proportion of Rab7-positive bacteria. HeLa cells expressing YFP-Rab7 and mCherry-Rab5 were infected with *S. aureus* JE2 for the indicated time point and extracellular bacteria were removed with lysostaphin for 15 min. Then, samples were fixed and imaged by CLSM. Proportion of bacteria associated with YFP-Rab7 was determined. n=5. **(B, C) Reduced association of *S. aureus* with Rab7 is not due to changes in phagosomal escape.** HeLa cells expressing YFP-Rab7 and the phagosomal escape marker RFP-CWT were treated with amitriptyline, PCK310 or β-toxin and subsequently, infected with *S. aureus* JE2 for 45 min and analyzed by CLSMs. Bacteria that escaped from phagosomes were subtracted from the data set and the proportion of residual bacteria associated with Rab7 was determined (C). Results of treated samples were normalized to untreated controls (B, n=7) . **(D) Phagosomal escape assay in early infection.** A HeLa reporter cell line expressing YFP-Rab7 and RFP-CWT was treated with amitriptyline, β-toxin and PCK310 and subsequently infected with *S. aureus* JE2 for 30 min. Extracellular bacteria were removed by lysostaphin and the

proportion of bacteria that acquired the phagosomal escape marker RFP-CWT was determined 45 and 60 min p.i. (n=8). **(E) β-toxin treatment and ASM inhibition reduced invasion efficiency of *S. aureus* JE2 in a dual reporter HeLa cell line.** A HeLa reporter cell line expressing RFP-CWT and Lysenin^{W20A}-YFP was treated with the indicated concentrations of β-toxin and amitriptyline for 75 min, the indicated concentrations of ARC39 for 22 h, 0.5 µM PCK310 for 4h or 50/100 nM PCK310 for 22h (o.n.) and invasion efficiency of *S. aureus* JE2 was determined. (n≥5) **(F) Inhibition of ASM has no influence on the proportion of Lysenin^{W20A}-positive escape events.** The dual reporter cell line was infected with *S. aureus* JE2. Extracellular bacteria were removed and the proportion of bacteria that acquired the phagosomal escape marker RFP-CWT as well as the SM reporter Lysenin^{W20A}-YFP was determined by CLSM. The proportion of escaped (RFP-CWT-positive) bacteria that additionally acquired Lysenin^{W20A}-YFP was calculated. (n=9). **(G) β-toxin pretreatment increases phagosomal escape of *S. aureus* JE2 but not *S. aureus* Cowan I.** RFP-CWT and Lysenin^{W20A} -YFP expressing HeLa were treated with 100 ng/ml β-toxin infected with *S. aureus* strains JE2 or Cowan I. Thereby, β-toxin was either removed prior to infection (pretreatment only) or was present during the whole experiment (pretreatment + during infection). By CLSM, proportions of bacteria that recruited RFP-CWT (phagosomal escape) were determined (n≥3). **(H) *S. aureus* strains vary in β-toxin expression.** The neutral SMase activity in culture supernatants of the indicated *S. aureus* strains or isogenic β-toxin mutants (Δ*hlb*) was determined by a TLC-based approach (n=3). **(I, J) β-toxin pretreatment of host cells but not β-toxin expression of endocytosed *S. aureus* affects phagosomal escape.** HeLa RFP-CWT/Lysenin^{W20A} -YFP were infected with *S. aureus* 6850 or an isogenic strain deficient in β-toxin production (Δ*hlb*). The proportion of bacteria that escaped from the phagosome (I) as well as the percentage of phagosomal escape events that were Lysenin^{W20A} -positive (J) were determined 3h p.i. (n=6). **(K) Increasing the MOI compensates for lower numbers of invading bacteria at shorter infection times.** HeLa cells were either infected for 10 min or 30 min with varying MOIs. Then, the number of intracellular bacteria per host cell was determined 3h p.i. by CLSM. (n=7). Statistics: One samples t-test (B, E), mixed effects analysis (REML) and Dunnett's multiple comparison (D), Two-way ANOVA with Tukey's multiple comparison (G), One-way ANOVA with Tukey's multiple comparison (H), mixed effects analysis (REML) and uncorrected Fisher`s LSD (I), mixed effects analysis (REML) with Šídák's multiple comparison (J).Bars represent mean +/- SD. *p≤0.05, **p≤0.01, ***p≤0.001, ****p≤0.0001.

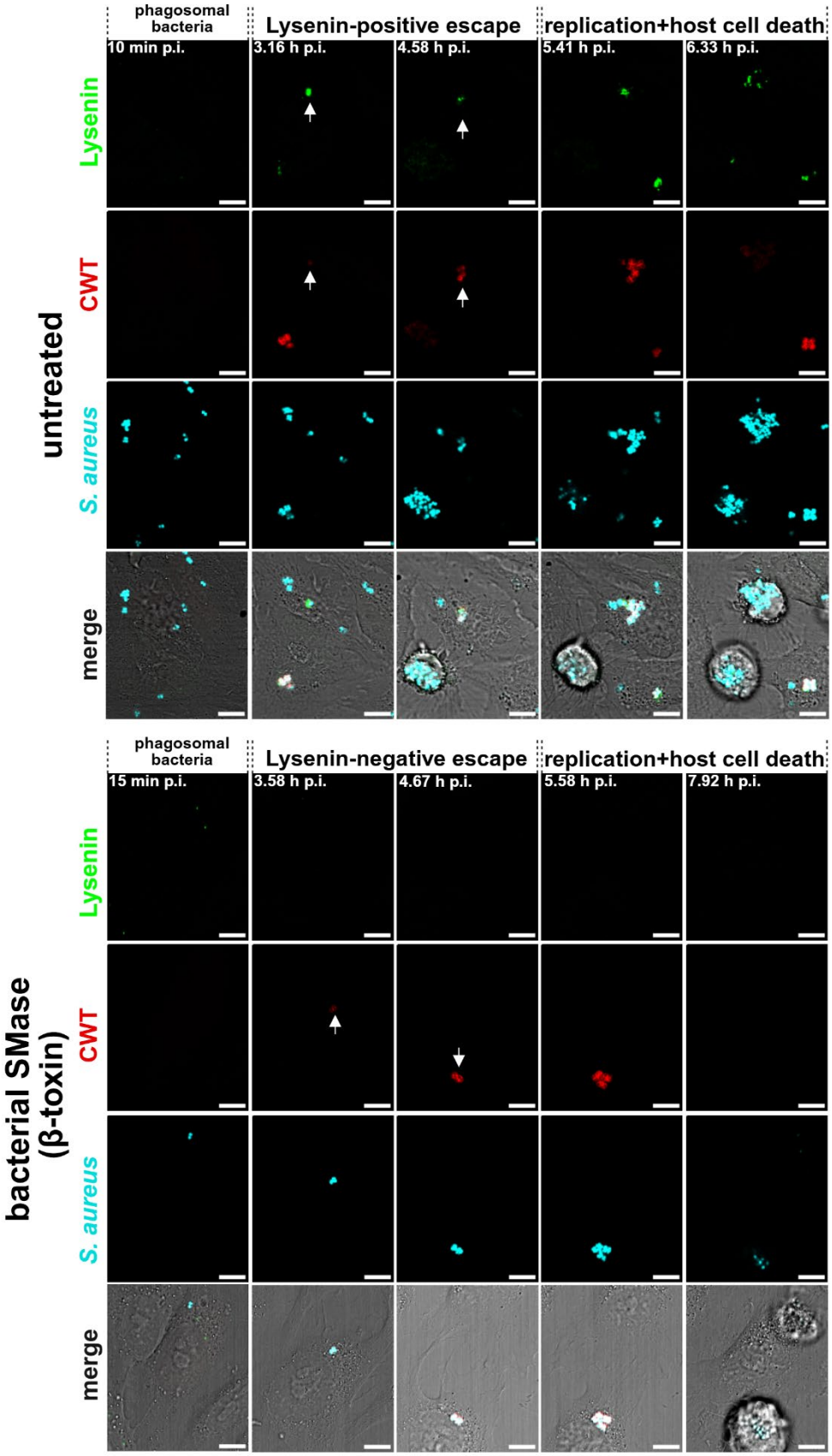

Supp. Figure 5 Validation of Lysenin^{W20A}-YFP and RFP-CWT reporter cell line

Hela cells expressing the SM reporter Lysenin$^{W20A\text{-}YFP}$(green) and the phagosomal escape reporter RFP-CWT (red) were either pretreated with 100 ng/ml bacterial SMase (A) or left untreated (B). Cells were infected with Cerulean-expressing *S. aureus* JE2 (cyan), extracellular bacteria were removed, and intracellular infection was monitored by time-lapse imaging at a Leica TCS SP5 microscope in 5 min intervals. White arrows indicate Lysenin-positive (A)or Lysenin-negative (B) escape events. Scale bars: 10 µm.

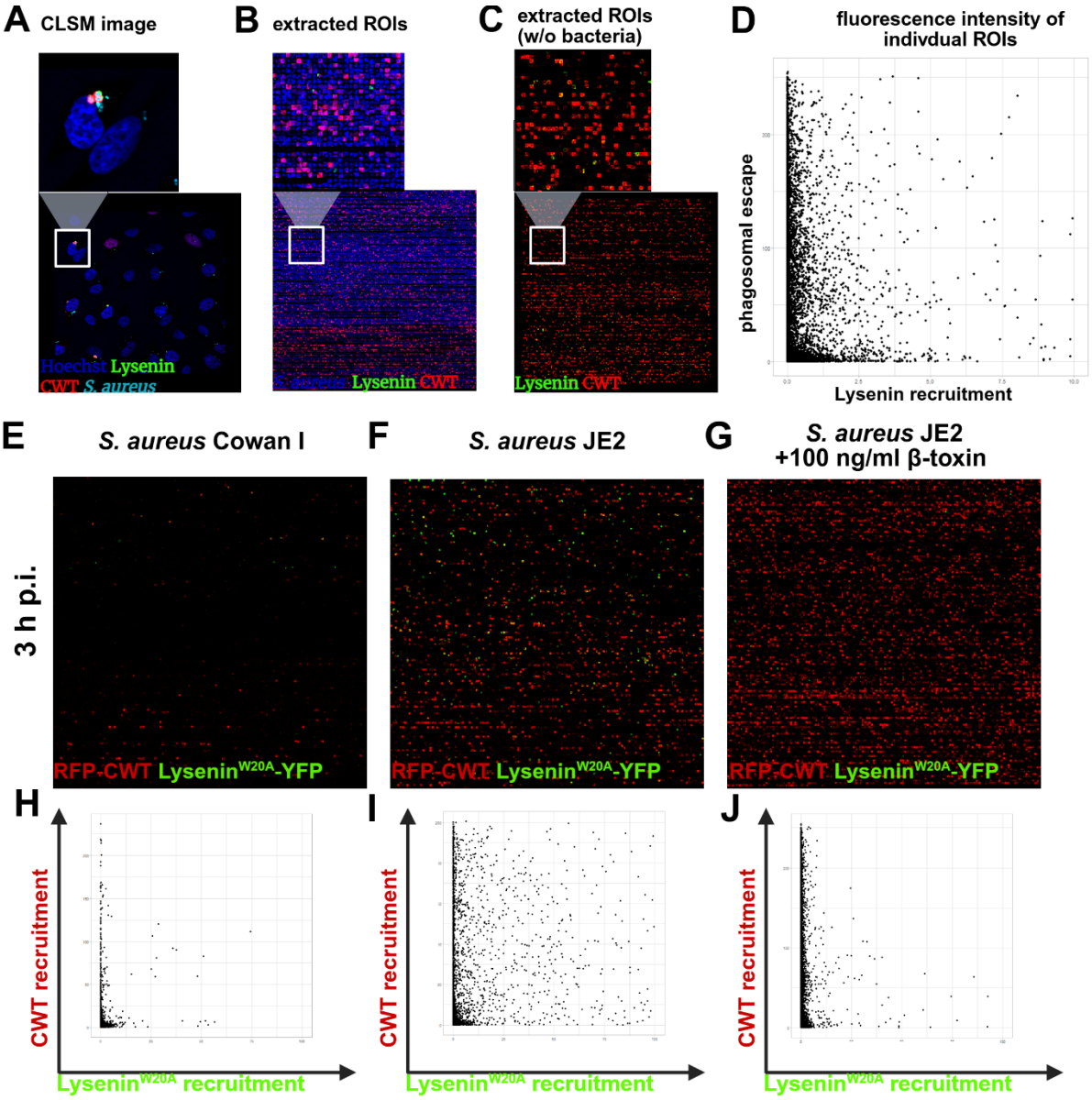

Supp. Figure 6 Evaluation of phagosomal escape and Lysenin^{W20A} recruitment during *S. aureus* infection. HeLa reporter cells expressing RFP-CWT and Lysenin^{W20A}-YFP were infected with *S. aureus* JE2, fixed and imaged by CLSM (**A**). Individual bacteria within the images were identified as regions of interest (ROIs) and extracted in each color channel. All extracted ROIs are depicted in a montage (**B**). If bacteria signals are omitted, the montage of extracted ROIs shows the proportion of reporter recruitment. The average fluorescence intensity of both reporter fluorophores is measured within each individual ROIs is plotted as dot plots (**D**). From these results, the proportion of bacteria that recruited the markers (CWT-RFP = phagosomal escape and Lysenin^{W20A} = SM-rich-phagosome) is calculated. **(E-J) Exemplary escape assay.** Montages of extracted ROIs (without bacterial fluorescence) as well as the resulting intensity measurement in individual ROIs 3 h p.i. are depicted for infections of *S. aureus* Cowan I (E, H) and JE2 (F, I) as well as an infection with *S. aureus* JE2 where host cells were treated with 100 ng/ml β-toxin prior to infection (G, J). Data are quantified in **Figure 4**, C.

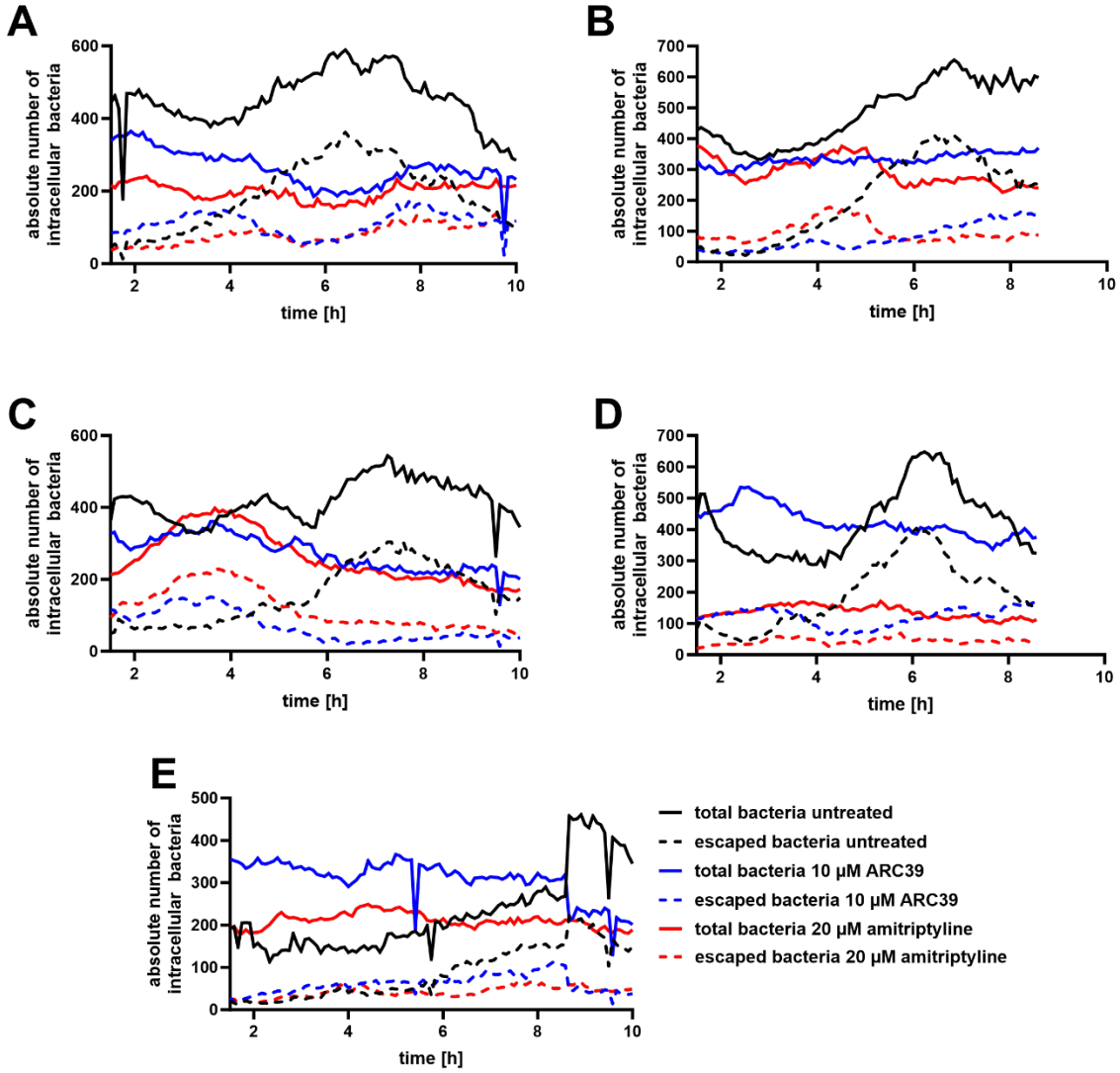

Supp. Figure 7 Individual replicates of time-dependent phagosomal escape and replication assays

HeLa cells expressing RFP-CWT were pretreated with 20 µM amitriptyline or 10 µM ARC39, infected with *S. aureus* JE2 and infection was monitored by live cell imaging (for further details see **Figure 6**, A and B). The absolute numbers of all intracellular bacteria and bacteria that escaped from the phagosome, which were detected during live cell imaging, are depicted.

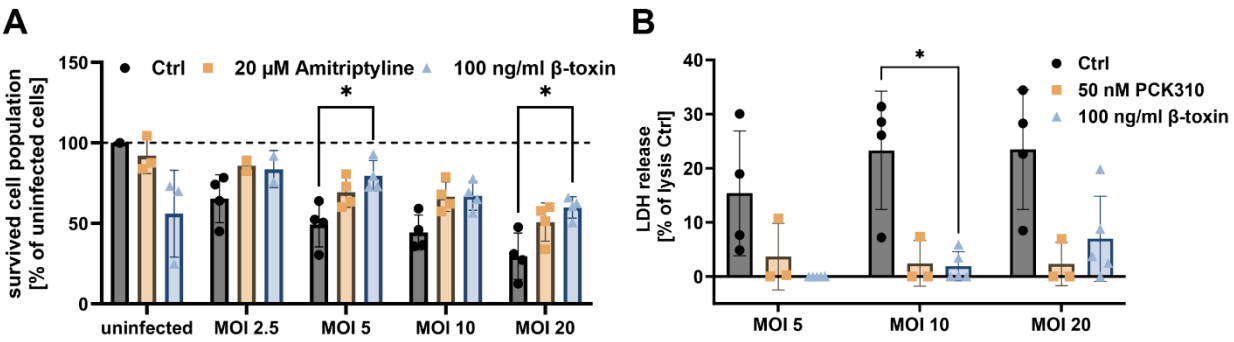

Supp. Figure 8 Inhibition of ASM and β-toxin treatment increase number of host cells remaining attached to the substratum and reduce host cell lysis during infection. HuLEC were treated with amitriptyline or β-toxin (**A**) or PCK310 and β-toxin (**B**) and were then infected with *S. aureus* JE2. After 30 min, extracellular bacteria were removed and the number of cells remaining attached to the substratum was determined (**A**) or the proportion of host cells that were lysed during the infection was measured by lactate dehydrogenase (LDH) release (**B**). Statistics: Mixed-effects analysis and Dunnett`s multiple comparison (A, B). Bars represent mean +/- SD. *p≤0.05, **p≤0.01, ***p≤0.001, ****p≤0.0001.

Supplementary Videos

Supp. Video 1 *S. aureus* associates with BODIPy-FL-C_{12}-sphingomyelin during invasion
(for further details, see Figure 3, A)

Supp. Video 2 *S. aureus* associates with a visible-range FRET probe during invasion
(for further details, see Supp. Figure 3)

Supp. Video 3 *S. aureus* associates with Rab5 and Rab7 upon host cell entry

Hela cells expressing mCherry-Rab5 (red) and YFP-Rab7 (green) were infected with fluorescent *S. aureus* JE2 (cyan). Time-laps imaging was performed at a Leica TCS SP5 microscope in intervals of 45 s. Scale bar: 10 µm.

Supp. Video 4 Validation of Lysenin and CWT reporter cell line

(for further details see Supp. Figure 5)

Supp. Video 5 Phagosomal Escape In Long Term Infection

(for further details see **Figure 6**, a)

Supp. Video 6 β-toxin pretreatment protects HuLEC from *S. aureus* infection
(for further details see Figure 6, c)